İSTANBUL TECHNICAL UNIVERSITY ★ INSTITUTE OF SCIENCE AND TECHNOLOGY

CHARACTERIZATION OF NiTi SHAPE MEMORY ALLOY FILMS PRODUCED BY MAGNETRON SPUTTERING

M.Sc. Thesis by

Ş. Murat TELLİ, B.Sc.

(706011009)

Date of submission : 26 April 2004

Date of defence examination: 21 May 2004

Supervisors (Chairman): Prof. Dr. Mustafa ÜRGEN

Prof. Dr. Yılmaz TAPTIK

Members of the Examining Committee: Prof.Dr. Ali Fuat ÇAKIR

Prof.Dr. Mehmet DEMİRKOL

Assis. Prof.Dr. Levent TRABZON

MAY 2004

İSTANBUL TEKNİK ÜNİVERSİTESİ ★ FEN BİLİMLERİ ENSTİTÜSÜ

MANYETİK ALANDA SIÇRATMA YÖNTEMİ İLE ÜRETİLEN NiTi HAFIZALI ALAŞIM FİLMLERİN KARAKTERİZASYONU

YÜKSEK LİSANS TEZİ
Met. Mal. Müh. Ş. Murat TELLİ
(706011009)

Tezin Enstitüye Verildiği Tarih : 26 Nisan 2004
Tezin Savunulduğu Tarih : 21 Mayıs 2004

Tez Danışmanları :	**Prof. Dr. Mustafa ÜRGEN**
	Prof. Dr. Yılmaz TAPTIK
Diğer Jüri Üyeleri :	**Prof. Dr. Ali Fuat ÇAKIR**
	Prof. Dr. Mehmet DEMİRKOL
	Yrd. Doç. Dr. Levent TRABZON

MAYIS 2004

ACKNOWLEDGEMENT

I would like to express my sincere gratitude to my advisors Prof. Dr. Mustafa ÜRGEN and Prof. Dr. Yılmaz TAPTIK for their support and guidance throughout this study. I am thankful for the knowledge and inspiration that they imparted to me during this research.

I would like to thank to M.Sc. Semih ÖNCEL and M.Sc. Ahmet ÖZTÜRK for their help in preparing the coatings.

I also would like to thank to Prof. Dr. Erdem DEMİRKESEN who has conducted my annealing experiments.

I would like to thank to Dr. Uğur DEMİRLER who has shortened my adaptation time to XRD studies by sharing knowledge with me.

I am really grateful to my friends ERDEM ARPAT, Tuncay TURUTOGLU, Bahadır KEPENEK and Ebru Devrim ŞAM for their endless support and help to me from the beginning of this study. Without their invaluable help and unique friendship, this study wouldn't have come into existence.

I would like to thank all of my friends who provided strength, motivation, confidence and moral support to me.

Finally, my biggest thanks go to my family for their love and support in every way.

May, 2004 Ş. Murat TELLİ

TABLE OF CONTENTS

ACKNOWLEDGEMENTS iii
TABLE OF CONTENTS iv
ABBREVIATIONS vi
LIST OF TABLES vii
LIST OF FIGURES viii
LIST OF SYMBOLS x
ÖZET xi
SUMMARY xiii

1. INTRODUCTION 1

2. SHAPE MEMORY ALLOYS 4
2.1. Nomenclature of Shape Memory Alloys 4
2.2. Shape Memory Phenomena 5
2.2.1. Martensitic Transformation 5
2.2.2. Shape Memory Effect 8
2.3. Stress-Induced Martensite and Superelasticity 11
2.3.1. Stress-Induced Martensite 11
2.3.2. Superelasticity 13
2.4. Two Way Shape Memory 14

3. NiTi BASED SHAPE MEMORY ALLOYS 17
3.1. Metallurgy of NiTi Alloys 17
3.2. Crystal Structures and Martensitic Transformation in NiTi 19
3.3. R-Phase Transition 19
3.4. Properties of NiTi Shape Memory Alloys 22
3.5. Measuring Transformation Temperatures 23
3.6. Corrosion Behavior of NiTi 24
3.7. Effects of Alloying Elements 25
3.8. Applications of NiTi Shape Memory Alloys 25

4. THIN FILM OF NiTi SHAPE MEMORY ALLOYS 27
4.1. Advantages of Using Thin Film NiTi 28
4.2. Shape Memory Thin Film Processing 28
4.3. Sputtering Introduction 29
4.4. Sputter Deposited Films of NiTi Alloys 30

5. EXPERIMENTAL **33**
5.1. Substrates 33
5.2. Preparation of Substrates 33
5.3. Thin Film Deposition 34
5.4. Compositional Analyses 34
5.5. Heat Treatment (Post-annealing) 35
5.6. X-Ray Diffraction Analyses 35
5.6.1. Phase Analyses 35
5.6.2. Transformation Experiments 36
5.7. Structural Analyses 36
5.7.1. Hardness Measurement 36
5.7.2. Thickness Measurement with XRF 37
5.7.3. Cross-section SEM Analyses 37

6. RESULTS AND DISCUSSION **38**
6.1. Compositional Analyses 38
6.2. Phase Analyses 39
6.2.1. KTF 638 NiTi film (300 W- 2 mTorr) 40
6.2.2. KTF 639 NiTi film (500 W- 2 mTorr) 41
6.2.3. KTF 640 NiTi film (300 W- 7,5 mTorr) 42
6.2.4. KTF 641 NiTi film (500 W- 7,5 mTorr) 44
6.2.5. Shifts in the Position of Peaks 45
6.2.6 Effect of Annealing Temperature on Crystallization and Transformation of the Films 46
6.2.7. Effect of Coating Parameters on Crystallization and Transformation of the Films 50
6.3. Structural Analyses 51
6.3.1. Hardness Measurement 51
6.3.2. Thickness Measurements with XRF 53
6.3.3. Cross-sectional SEM Analyses 54

7. CONCLUSION **58**

REFERENCES **60**

APPENDIX **65**

RESUME **75**

ABBREVIATIONS

SMA	: Shape Memory Alloy
SME	: Shape Memory Effect
DSC	: Differential Scanning Calorimeter
TTRs	: Transformation Temperatures
SIM	: Stress-Induced Martensite
NOL	: Naval Ordnance Laboratory
BCC	: Body Centered Cubic
MEMS	: Micro-Electro-Mechanical Systems
DC	: Direct Current
RF	: Radio Frequency
PVD	: Physical Vapor Deposition
EDS	: Energy Dispersive Spectrometry
XRD	: X-Ray Diffraction
JCPDS	: Joint Committee on Powder Diffraction Standards
XRF	: X-Ray Fluorescence
SEM	: Scanning Electron Microscope

LIST OF TABLES

		Page
Table 2.1.	Some alloy systems exhibiting the shape memory effect.....	11
Table 3.1.	Selected Properties of NiTi.....	22
Table 5.1.	Conditions for the deposition of NiTi thin films.....	34
Table 5.2.	Annealing conditions for the as-deposited NiTi thin films.....	35
Table 5.3.	The conditions for the XRD experiments.....	36
Table 6.1.	The results of compositional analyses belonging to deposited films.....	38
Table 6.2.	The hardness measurement results of the films.....	52
Table 6.3.	Thickness of the films determined by XRF and cross-sectional SEM micrographs.....	53
Table B.1	JCPDS of NiTi with Reference File No of 18-0899.....	68
Table B.2	JCPDS of NiTi with Reference File No of 19-0850.....	69
Table B.3	JCPDS of NiTi with Reference File No of 35-1281.....	70
Table B.4	JCPDS of NiTi with Reference File No of 27-0344.....	71
Table B.5	JCPDS of Ti_2Ni with Reference File No of 18-0898.....	72
Table B.6	JCPDS of Ni_3Ti with Reference File No of 05-0723.....	73
Table B.7	JCPDS of Ni_4Ti_3 with Reference File No of 39-1113.....	74

LIST OF FIGURES

		Page
Figure 2.1	: The transformation from austenite to martensite a) completely austenite, d) completely martensite.....	6
Figure 2.2	: The two mechanisms of accommodating the shape change due to the atomic shear of a martensitic transformation, a) accommodation by slip, b) accommodation by twinning.....	7
Figure 2.3	: Ordered and disordered structures that are commonly found in SMAs. (a) Disordered BCC structure, (b) B2 structure, (c) highly ordered state DO_3.....	8
Figure 2.4	: Hypothetical plot of property change vs. temperature for a martensitic transformation occurring in a SMA.....	8
Figure 2.5	: A simplified model martensitic transformation which is diffusionless phase transformation.....	9
Figure 2.6	: The microscopic shape memory process.....	10
Figure 2.7	: The SME is described with a reference to a plot of electrical resistance vs. temperature from which the characteristic transformation temperatures M_s, M_f, A_s and A_f are determined.	10
Figure 2.8	: Stress-strain curves for a Cu-Zn single crystal loaded in tension above M_s. As the M_s temperature is approached, the stress required to induce martensite is lowered.....	12
Figure 2.9	: The linear plot which obeys the Clasius-Clapeyron equation..	12
Figure 2.10	: Stress-strain curve for a Cu-Zn shape memory alloy loaded above the A_s temperature and then unloaded shows distinct superelastic behavior. SIM is formed during loading, which becomes unstable and disappears upon loading.....	13
Figure 2.11	: Comparison of springs made of superelastic SMA and conventional piano wire.....	14
Figure 2.12	: Comparison of the one-way (upper) and two-way (lower) shape memories using a coil spring as an example.....	15
Figure 2.13	: Illustration of several training routines that can be used to produce two-way shape memory behavior.....	15
Figure 3.1	: Binary Phase diagram of NiTi.....	17
Figure 3.2	: The dependence of the transformation temperature M_s on composition.....	18
Figure 3.3	: B2 to B19` transformation, Top: Crystal structure before the transformation, a tetragonal cell in B2 matrix is delineated. Bottom: the transformed monoclinic cell. Tetragonal cell before the transformation is shown with the dashed line. The axis x_1, x_2, x_3 are along the cube axis, the axis z_1, z_2, z_3 are along the tetragonal axis.....	20
Figure 3.4	: Rhombohedral lattice of the R-Phase.....	21

Figure 3.5 : Specimen length vs. Temperature in a Constant Load Test of NiTi..... 23
Figure 3.6 : A typical DSC curve for a NiTi SMA..... 24
Figure 4.1 : Electron diffraction patterns of NiTi alloy thin film..... 31
Figure 4.2 : Elongation-temperature curve of a sputter deposited Ti-51,6 % Ni alloy film..... 32
Figure 6.1 : XRD patterns obtained for KTF 638 films produced at 300 W- 2 mTorr P_{Ar} and annealed at different temperatures..... 40
Figure 6.2 : XRD patterns obtained for KTF 639 films produced at 500 W- 2 mTorr P_{Ar} and annealed at different temperatures..... 42
Figure 6.3 : XRD patterns obtained for KTF 640 films produced at 300 W- 7,5 mTorr P_{Ar} and annealed at different temperatures..... 43
Figure 6.4 : XRD patterns obtained for KTF 641 films produced at 500 W- 7,5 mTorr P_{Ar} and annealed at different temperatures..... 44
Figure 6.5 : Shifts in peak positions of KTF641 films produced at 500 W- 7,5 mTorr P_{Ar}..... 46
Figure 6.6 : The crystallization behaviors of the films deposited under different conditions and annealed at 550 °C..... 47
Figure 6.7 : The crystallization behaviors of the films deposited under different conditions and annealed at 700 °C..... 48
Figure 6.8 : The crystallization behaviors of the films deposited under different conditions and annealed at 775 °C..... 49
Figure 6.9 : Hardness of the films for as-deposited states and annealed at different temperatures..... 51
Figure 6.10 : Cross-sectional micrographs of KTF638 film produced at 300W- 2 mTorr P_{Ar}..... 54
Figure 6.11 : Cross-sectional micrographs of KTF639 film produced at 500W- 2 mTorr P_{Ar}..... 55
Figure 6.12 : Cross-sectional micrographs of KTF 640 film produced at 300W- 7,5 mTorr P_{Ar}..... 56
Figure 6.13 : Cross-sectional micrographs of KTF 641 film produced at 500W- 7,5 mTorr P_{Ar}..... 57
Figure A.1 : Transformation experiments of KTF638 (300 W – 2 mTorr) films at 70 °C for different annealing temperatures..... 65
Figure A.2 : Transformation experiments of KTF639 (500 W – 2 mTorr) films at 70 °C for different annealing temperatures..... 66
Figure A.3 : Transformation experiments of KTF640 films (300 W- 7,5 mTorr) at 70 °C for different annealing temperatures..... 66
Figure A.4 : Transformation experiments of KTF641 (500 W- 7,5 mTorr) films at 70 °C for different annealing temperatures..... 67
Figure A.5 : Magnified scheme of XRD patterns of KTF 641 (500 W- 7,5 mTorr) films compared with the original peak positions of B2 and B19` phases..... 67

LIST OF SYMBOLS

M_s, M_f, M_p,M_d	: TTRs of martensite
A_s, A_f, A_p	: TTRs of austenite
R_s, R_f	: TTRs of R-phase
P	: Pressure
T	: Temperature
ΔH	: Transformation latent heat
σ	: Stress
ε_0	: Transformational strain
E	: Young's modulus
υ	: Poisson's ratio

MANYETİK ALANDA SIÇRATMA YÖNTEMİ İLE ÜRETİLEN NiTi HAFIZALI ALAŞIM FİLMLERİN KARAKTERİZASYONU

ÖZET

Hafızalı alaşımlar, ısıtıldıklarında önceden belirlenmiş şekillerine dönebilen malzemelerdir. Bu alaşımlar düşük sıcaklıklarda sünek ve kolayca deforme edilebilen martenzit faz yapısındadırlar. Martenzit fazında iken deforme edilmiş malzeme yüksek sıcaklıklara çıkarıldığında, malzemenin faz yapısı ostenite dönüşür ve düşük sıcaklıkta uygulanmış olan deformasyon da tam anlamıyla toparlanır. Bu malzemeler hafıza etkisinin yanı sıra süperelastik özellik de gösterirler. Bu özellik, malzemenin ostenit faz yapısında iken deforme edilmesi ile oluşur. Bu malzemeye bu halde iken soğutma yapmaksızın sadece deformasyon uygulandığında malzeme bu etkiyle büyük bir deformasyon altında martenzit faz yapısına geçer ki, oluşan bu yapıya gerilme-katkılı martenzit olarak adlandırılır. Hafızalı alaşımlarda toparlanabilir deformasyon % 10 mertebelerindedir.

Hafizalı alaşımlarda; M_s- martenzit başlangıç sıcaklığı, M_f- martenzit bitiş sıcaklığı, A_s- ostenit başlangıç sıcaklığı ve A_f- ostenit bitiş sıcaklığı olmak üzere faz dönüşümü boyunca gözlenen dört önemli sıcaklık mevcuttur. Bu sıcaklıklar o malzemeye ait faz sınırlarını gösterirler.

Hafıza özelliğine bağlı olarak hafızalı alaşımlar iki şekilde sınıflandırılırlar. Bunlardan birincisi "tek yönlü hafıza" olarak adlandırılır ve bu özellikteki hafızalı alaşım, ostenit sıcaklığına çıkarıldığında deformasyonu toparlamasına rağmen soğutulduğunda ostenit fazında iken bulunduğu şeklini muhafaza eder. İkincisi ise "çift yönlü hafıza" olarak adlandırılır. Bu özellikteki hafızalı alaşımlar, düşük ve yüksek sıcaklıklarda faz dönüşümüne paralel olarak şekil dönüşümü de gösterirler.

Sıçratma yöntemi ile üretilen NiTi hafızalı alaşım ince filmler, mikroelektromekanik sistemlerde (MEMS) katı hal aktive edicisi olarak kullanılabilecek yeni bir malzeme tipi oluştururken, tıp alanında da bu önemde benzer kullanım sahaları oluşturmuştur. Kitlesel hafızalı alaşımlar büyük darbe ve yük dayanımına karşılık, çok düşük frekanslı bir tepki mekanizmasına sahiptirler. İnce film hafızalı alaşımlar yüksek enerji yoğunluğuna, yüksek frekanslı tepki mekanizmasına ve uzun kullanım ömrüne sahip olmalarıyla dikkat çekmişlerdir. Ancak, özellikle NiTi hafızalı alaşımları için (1) malzeme özelliklerinin kontrolünde yaşanan zorluklar, (2) diğer MEMS malzemeleriyle üretim aşamasındaki uyum problemleri, NiTi hafızalı alaşım ince filmlerin MEMS alanında hala yeteri kadar kullanım sahası bulamamasına neden olmaktadır.

Hafızalı alaşım ince filmler değişik yöntemlerle üretilebilmektedir. Bunların başlıcaları: buharlaştırma, soğuk hadde, vakum plazma püskürtme ve iyon sıçratma yöntemleridir. Ancak, en fazla kullanılan yöntem sıçratma yöntemidir. Özellikle istenen kalınlık ve kimyasal bileşimin sağlanabilmesi açısından manyetik alanda sıçratma bir adım öne çıkmaktadır.

Bu çalışmada, doğru akım manyetik alanda sıçratma yöntemiyle hızlı takım çeliği (HSS) taban malzemeler üzerine NiTi hafızalı alaşım ince film biriktirilmiştir. Deneylerde Ar basıncı ve hedef malzeme gücü değiştirilerek (2 ve 7,5 mTorr Ar basıncı – 300 ve 500 W hedef malzeme gücü) bu parametrelerin filmlerin kristalizasyonu ve faz dönüşümleri üzerindeki etkisi incelenmiştir. Kaplama sonrası filmlerin amorf yapıda olması sonucu bu filmler 500, 700 ve 775 ^{o}C gibi üç farklı sıcaklıkta ve 10^{-3}-10^{-4} mTorr mertebelerindeki yüksek vakum değerlerinde tavlanmışlardır. Kaplama parametreleri gibi, tavlama sıcaklıklarının da film kristalizasyonu ve faz dönüşümü üzerindeki etkileri incelenmiştir.

Üretilen filmlerin bileşimlerine değiştirilen kaplama parametrelerinin etkisi incelenmiş olup artan hedef malzeme gücü ve argon basıncının filmlerdeki Ti içeriğini arttırdığı saptanmıştır.

Üretilen filmlere ait faz ve dönüşüm özellikleri XRD yöntemi ile incelenmiştir. Bu sayede tavlama sıcaklığının filmlerin kristalizasyonu ve dönüşümleri üzerindeki etkisi belirlenmiştir. Buna göre, belirlenen üç tavlama sıcaklığı içinde 700 ^{o}C'de yapılan tavlamaların sonucunda filmler, ana yapılarının ikincil çökelti fazlarından oluştuğu bir şekilde kristalin hale gelmişlerdir. 550 ve 775 ^{o}C'de yapılan tavlamalar sonucunda, değişen oranlarda olmak kaydıyla, filmler, ana yapının B2 ostenit ve B19` martenzit fazından oluştuğu, bunlara ilaveten ise ikincil çökelti fazlarının bulunduğu benzer kristalizasyon davranışları sergilemişlerdir. 550 W- 7,5 mTorr koşullarında üretilen ve 775 $^{o}$C'de tavlanan filmde ise diğerlerinden farklı olarak tavlama sonucu oda sıcaklığında B19` martenzit fazının ana faz olarak yer aldığı bir kristalizasyon ortaya çıkmıştır. Oda sıcaklığında martenzit fazının ana faz olarak oluşması, bu filme ait dönüşüm sıcaklıklarının üretilen diğer filmlerden kalitatif anlamda daha yüksek olduğunu göstermektedir.

Filmlere ait sertlikler ultra mikrosertlik cihazi ile belirlenmiştir. İkincil çökelti fazlarının ana faz olarak yapısında yer aldığı filmlerin sertlikleri diğerlerine nazaran yüksek çıkmıştır. Film kalınlıkları X-ışınları floresan radyasyonu yöntemi ile belirlenmiş, taramalı elektron mikroskobunda yapılan kırık yüzey morfolojilerinin incelenmesi aşamasında ise bu kalınlık değerleri doğrulanmıştır. Buna göre, hedef malzeme gücü ve argon basıncının artmasıyla film kalınlıklarında artış gözlenmiştir. Filmlere ait kırık yüzey morfolojileri yapılar hakkında genel bir fikir vermezken, 500 W- 7,5 mTorr'da üretilen film için artan tavlama sıcaklığına bağlı olarak yapının kolonsal hale dönüştüğü gözlenmiştir.

CHARACTERIZATION OF NiTi SHAPE MEMORY ALLOY FILMS PRODUCED BY MAGNETRON SPUTTERING

SUMMARY

The term shape memory alloy (SMA) refers to a material, which returns to a predetermined shape when heated. At low temperature, the phase of SMA material is martensite, which is ductile and can be deformed easily. However, by simply heating the deformed material to an elevated temperature, the material's phase changes to austenite and the deformation induced at lower temperature can be fully recovered. These materials also exhibit superelasticity. This behavior occurs when the material is deformed in the austenite phase. By applying stress, the phase of the material changes to martensite which is called as stress-induced martensite (SIM). When the stress is released, the phase returns to austenite without any permanent deformation. Recoverable strains in SMAs are up to 10%.

There are four distinctive temperatures for SMA: M_s-martensite starting temperature, M_f- martensite finishing temperature, A_s- austenite starting temperature, and A_f- austenite finishing temperature. These temperatures represent the phase boundary.

There are two general classes of SMA material depending on its ability to remember a shape. The former is the one-way effect which describes SMA's ability to recover deformation when heated to austenite, but to retain the hot shape when cooled down to martensite. The latter is the two-way effect that describes SMA ability to achieve two stable shapes. Therefore, the shape memory can occur between the two predetermined low and high temperature shapes.

NiTi SMA thin films produced by sputtering offers a promising new material for solid state actuation in the MEMS field as well as new possibilities for medical devices. Bulk SMAs exhibit large strokes and forces but suffer from slow response. However, thin film SMAs provide a larger energy density, higher frequency response and longer life time at the microscale. But, the reasons; (1) difficulty in controlling the material properties, and (2) fabrication compatibility with other MEMS materials, impede the widespread use of NiTi thin films for MEMS applications.

There are various methods to deposit SMA thin film, for example evaporation, laser ablation deposition, cold rolling, vacuum plasma spray, ion sputter deposition. However, most widely used deposition technique is sputtering. Magnetron sputtering is believed to be the simplest and most reliable method to produce shape memory thin films with desired thickness and composition.

In this study, NiTi thin films on HSS substrates were produced with DC magnetron sputtering method. The experiments were conducted under different Ar pressures (2 and 7,5 mTorr) and target powers (300 and 500 W). Effects of Ar pressure and target power on crystallization and phase transformation of NiTi films were investigated. Because as-deposited films were amorphous, they were annealed at three different temperatures of 550, 700 and 775 ^{o}C under high vacuum. The applied vacuum values

were in the range of 10^{-3}-10^{-4} mTorr. Effects of annealing temperature on crystallization and phase transformation of NiTi films were investigated.

The composition of the films were determined in order to observe the effect of target power and argon pressure on the composition. The results showed that Ti content of the films increased with increasing target power and argon pressure.

Phase and transformation analyses of different temperature annealed films were conducted by XRD method. Effects of the annealing temperature on the crystallization and transformation of the films were determined. Among three annealing temperatures, films annealed at 700 °C resulted with the crystallization of second phase precipitates as the major phases. With varying amounts, annealing at 550 and 775 °C showed formation of B2 austenitic and B19` martensitic phases as the major phases with second phase precipitates beside them. For the film produced at 550 W- 7,5 mTorr and annealed at 775 °C showed B19` martensitic phase as the major phase at room temperature showing that increase in annealing temperature, increased the TTRs of the film qualitatively.

Hardness of the films were measured by ultra micro hardness tester. Films with second phase precipitates as the major phases showed the highest hardness. The thickness of the films were measured with XRF method. Results of thickness measurement were verified with cross-sectional visualization of the films. Increase in target power and argon pressure increased the thickness of the films. Cross-sectional morphologies of the films did not give uniform idea about the film morphology except the film produced at 500 W- 7,5 mTorr which showed columnar structure with increasing annealing temperature.

1. INTRODUCTION

As a definition, shape memory alloys (SMAs) are metallic materials which are able to return to their original shapes when heated or cooled under the effect of shape memory (SME) [1-3]. Recoverable strains in SMAs are up to 10% [2]. If SME is seen only when the SMAs are heated, then they are said to have a "one-way shape memory". In addition to previous expression, if this effect is still seen on subsequent cooling, then these materials are said to have a "two-way shape memory", for which the recoverable strain is limited to about 3% [2-5].

SMAs are particularly useful materials; because they have a rubbery behavior at low temperatures and can be deformed easily by a small force, whereas at high temperatures, they behave like normal metals and any induced strain is not recoverable [5]. SMAs also exhibit superelasticity (or pseudo elasticity). A small force induces considerable deformation on these materials but when the force is removed, the material automatically recovers its original shape without the need for heating [2,3,6].

Although SMAs have been around for many years, people are often unaware of their presence and functions. One of the revealed applications is in 'indestructible' spectacle frames which can be bent and twisted to a remarkable extent and then regain their original shape [7].

Generally, a relatively wide variety of alloys are known to exhibit the SME, but only the ones that can recover high amounts of strain or that generate considerable force upon changing shape, attract the commercial interest. To date, this has been the nickel-titanium alloys and copper-base alloys such as CuZnAl and CuAlNi [5].

The first observations of the shape memory started with Chang and Read in 1932 on AuCd about reversibility of the transformation by metallographic observations and resistivity changes. In 1938, the transformation was seen in brass (CuZn) [5]. To date, SMAs based on nickel and titanium (NiTi) have provided the best combination of material properties for the most commercial applications due to their combination of material properties, stability, good corrosion resistance as well as biocompatibility

[8-12]. Buehler and co-workers discovered the SME effect in equiatomic nickel-titanium (NiTi) in 1962 [8]. This discovery accelerated the use of these materials in practical applications. The Naval Ordnance Laboratory (NOL) was the first place where NiTi was discovered. Therefore, the name NiTi-NOL or Nitinol is generally used when referring to NiTi based SMAs [8,11]. Today, studies about SMAs have come to an important point; more products using these materials are coming to the market each year [5].

On the other hand, NiTi thin films produced by sputtering offers a promising new material for solid state actuation in the MEMS field as well as new possibilities for medical devices [13]. Bulk SMAs exhibit large strokes and forces but suffer from slow response. However, thin film SMAs provide a larger energy density, higher frequency response and longer life time at the microscale [14].

Because of its large energy density (1 j/g) and large displacement (10% recoverable strain), thin film NiTi is highly appropriate for micro-actuation [15-17]. Beside these, the frequency response of NiTi is considerably improved at the microscale. Though NiTi is a promising actuator, there are some difficulties with depositing of this film that impede the widespread use of the material.

Walker et al. was the first group to incorporate thin film NiTi with a micromachining process in 1990. However, their films were amorphous. In 1990, Bush and Johnson at the TiNi Alloy Company showed the first definitive evidence of the SME in NiTi films [16]. Heat actuating property of NiTi SMAs makes them usable at microscales. With their smaller mass and larger surface to volume ratio, heat transfer is significantly increased, power requirements are lowered, and therefore, large stresses and strains are achievable. These advantages make NiTi SMA a very promising actuator material for microdevices such as microvalves, microgrippers, micropumps, micro-robotic applications [13].

Shape memory films can be produced in different ways such as cold rolling, vacuum plasma spray, ion sputter deposition and DC or RF magnetron sputtering. Among them, magnetron sputtering is believed to be the simplest and most reliable method to produce shape memory thin films with desired thickness and composition. However, sputtering of NiTi thin film from a 50/50 at% NiTi alloy target produces films with transformation temperatures different from the target due to loss of Ti

during process. Although this fact makes its use as an actuator questionable, researchers overcame this problem by placing Ti plates on the target as a multi target system or by using non-equiatomic Ti-rich targets [9-11].

The aim of this study was to produce thin films of shape memory NiTi alloy by magnetron sputtering and to investigate their phase transformation behavior with XRD technique. For this purpose, SMA NiTi thin films were deposited under different target power and argon pressure conditions. The amorphous as-deposited films were post-annealed at different temperatures. The effect of different deposition parameters and annealing temperatures on the crystallization and phase transformation behavior of the films were investigated.

2. SHAPE MEMORY ALLOYS

2.1. Nomenclature of Shape Memory Alloys

One must be familiar with the expressions below before starting to deal with SMAs;

A_f Temperature: The temperature at which a SMA finishes transforming to Austenite upon heating.

A_p Temperature: The temperature at which a SMA is about 50% transformed to Austenite upon heating, as measured by the peak on a DSC curve.

A_s Temperature: The temperature at which a SMA transforming to Austenite upon heating.

Alloy Phase: A particular arrangement of atoms (or crystal structure) in an alloy.

Austenite: The stronger, higher temperature phase present in SMA.

Biocompatibility: A general term used to describe the suitability of a material for exposure to the body or bodily fluids. The specific meaning is dependent upon the particular application or circumstances.

DSC : A Differential Scanning Calorimeter used to measure the phase transformation temperatures in SMAs by detecting the changes in heat flow in the alloy during phase transformation.

Hysteresis: The temperature difference between a phase transformation upon heating and cooling. In NiTi alloys, it is generally measured as the difference between A_p and M_p.

M_f Temperature: The temperature at which a SMA finishes transforming to Martensite upon cooling.

M_p Temperature: The temperature at which a SMA is about 50% transformed to Martensite upon cooling, as measured by the peak on a DSC curve.

M_s Temperature: The temperature at which a SMA starts transforming to Martensite upon cooling.

Martensite: The more deformable, lower temperature phase present in SMA.

Phase Transformation: The change from one alloy phase to another with a change in temperature, pressure, stress, chemistry, and/or time.

R-Phase: An intermediate phase between Martensite and Austenite that can form in NiTi SMAs under certain conditions.

Shape Memory: The ability of certain alloys to return to a predetermined shape upon heating via a phase transformation.

Superelasticity: The springy, "rubberlike" behavior present in NiTi SMAs at temperatures just above the A_f temperature. The superelasticity arises from the formation and reversion of stress-induced martensite.

Thermo-elastic Martensitic Transformation: A diffusionless, thermally reversible phase transformation characterized by a crystal lattice distortion [18].

2.2. Shape Memory Phenomena

The shape memory alloys are quite fascinating materials due to their shape memory effect and superelasticity, which are not present in ordinary metals and alloys [3].

2.2.1. Martensitic Transformation

It means ability of "remember" a shape when saying shape memory, even after rather high amount of deformations. Once, when SMAs are deformed at low temperature in their martensitic phase, they stay deformed until they are heated. After heating, they spontaneously return to their original, undeformed shape [2]. The memory effect in these materials based upon the fact that they can easily transform to and from martensite, which is a type of solid state transformation [19]. Solid state transformations are seperated into two types which are diffusional and displacive, respectively.

A new phase can only be formed by moving atoms randomly over relatively long distances for the diffusional type of transformations. Atomic migration is required in diffusional type of transformation. Therefore, the progress for this type of transformation is both time and temperature dependent. On the other hand, displacive transformations do not require such long range movements like in diffusional transformation. Displacive transformation is based on the rearrangement of the atoms

into a new, more stable crystal structure without changing the chemical nature of the matrix. Due to the absence of atomic migration, displacive transformations are generally time-independent cases. Martensitic transformations are generally of this second type, and are formed upon cooling from a higher temperature phase called the parent phase, or austenite [2].

Martensitic transformations are first order transformations. That means, heat is released when martensite is formed. There is also a hysteresis associated with transformation, and there is a temperature range in which austenite and martensite exist together [1,2,19,20].

Crystallographically, Bain Strain and Lattice Invariant Shear are the two parts taking role in the mechanism of transformation from austenite to martensite. These can be crystallographically quite complex. However, a qualitative two-dimensional approach makes it simple to be understood. Simply, the Bain Strain or lattice deformation consists of all the atomic movements needed to produce the new structure from the old. Figure 2.1 illustrates the progression of the transformation from the austenite structure to martensite structure. As the interface progresses one atomic layer, each atom is required to move only a very small amount. [2]

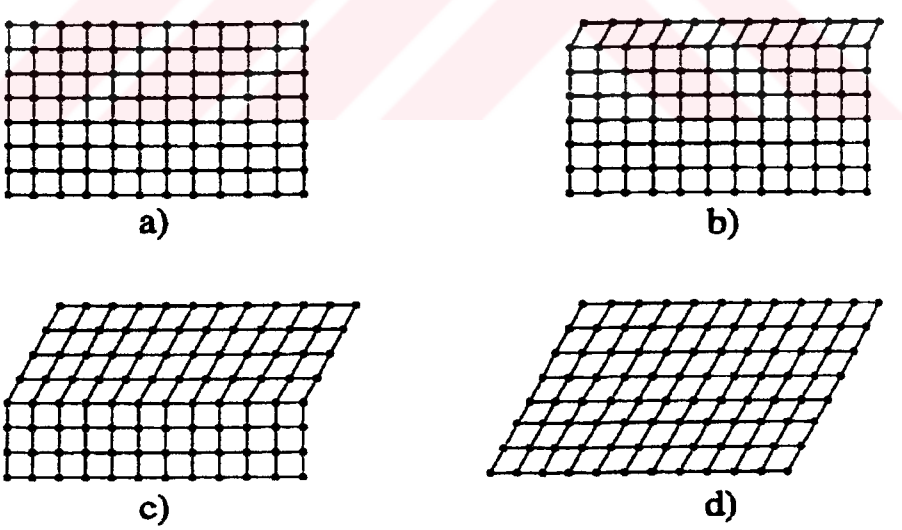

Figure 2.1 The transformation from austenite to martensite a) completely austenite, d) completely martensite [1].

The lattice invariant shear is an accommodation step with the formed martensitic structure by the bain strains of a different shape and volume than the surrounding austenite. While martensite in steel undergoes both a volume and a shape change, SMAs usually involve basically only a shape change. This change can happen in two

general mechanisms; slip and twinning as seen in Figure 2.2. In both cases, although the overall shape is that of the original austenite, each individual cell has the new martensitic structure. Slip is a permanent process and is a common accommodation in many martensites. Twinning is unable to accommodate volume changes but can accommodate shape changes in a reversible way. For the shape memory to occur, it is required that the accommodation be fully reversible, or that twinning be the dominant accommodation process.

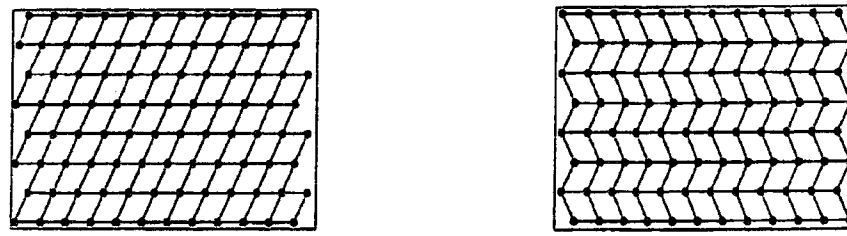

Figure 2.2 The two mechanisms of accommodating the shape change due to the atomic shear of a martensitic transformation, a) accommodation by slip, b) accommodation by twinning [1].

The twinning process of accommodation has an important role in the SME. From Figure 2.2, it can be noticed that slip accommodation requires that atomic bonds be broken, whereas all bonds remain intact in the twinned structure.

In Figures 2.1 and 2.2, atom types are the same, but we know that in an alloy, several species of atoms are present. How these atoms distribute themselves on the lattice sites must also be discussed on. In steel, atoms are disordered meaning that different elements are randomly distributed on the lattice sites. But in NiTi, atoms are ordered which means that Ni and Ti atoms are found on very specific sites. The distribution of atoms themselves to the lattice sites can be seen in Figure 2.3. Structures shown in Figure 2.3 have a body centered symmetry, technically Figure 2.3b is not BCC since the atoms at the corners are different in nature to those at the center, but is called a B2 structure or CsCl structure. SMAs are generally based upon a BCC symmetry, some with the BCC structure, more often with the B2 structure (NiTi) and some with an even more complex ordering called DO_3 (CuAlNi), still based upon a BCC symmetry (Figure 2.3c). [2]

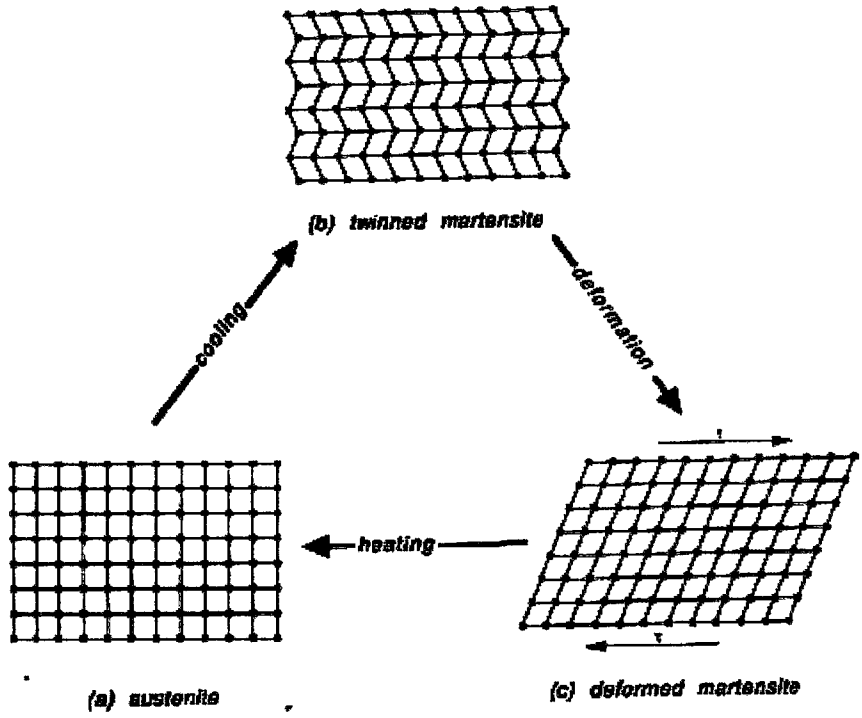

Figure 2.6 The microscopic shape memory process [2].

The SME can be described with reference to the cooling and heating curves in Figure 2.7. When the specimen is cooled from A_f to below M_f, there is no change in the shape. If the specimen is deformed at this point, it remains so deformed until it is heated. At the inflection point between A_s and A_f, about 50% of the original shape is recovered.

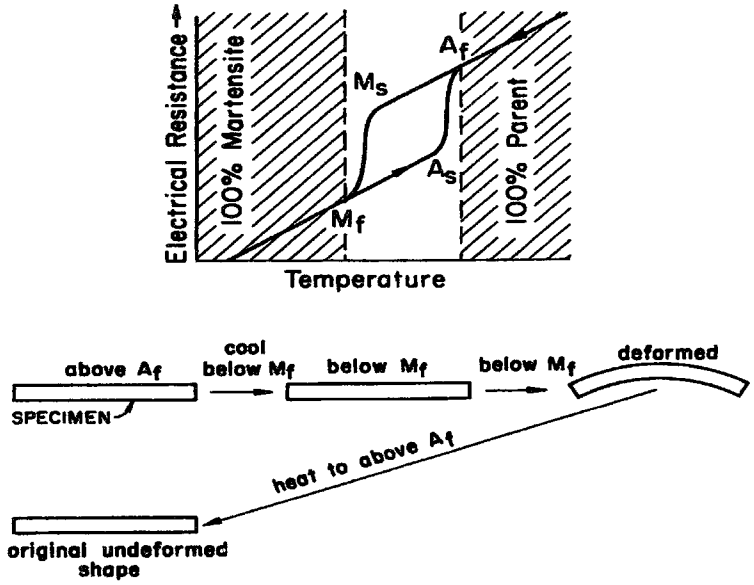

Figure 2.7 The SME is described with a reference to a plot of electrical resistance vs. temperature from which the characteristic transformation temperatures M_s, M_f, A_s and A_f are determined [2].

The SME is a one time only occurrence and because of this, it is frequently referred to as one-way shape memory. Even though the recoverable strains on the order of 7% are typical of SMAs, some of them show recoveries as high as 10%. [2]

Table 2.1 shows the alloys exhibiting the SME. Of these alloys shown, only CuZnAl, CuALNi and NiTi alloys are presently of commercial importance.

Table 2.1 Some alloy systems exhibiting the shape memory effect [2,3]

Alloy	Austenite Structure	Alloy	Austenite structure	Alloy	Austenite structure
Au-Cd	B2	Au-Cu-Zn		Cu-Zn-Ga	B2
Cu-Zn	B2	Cu-Zn-Sn	B2	Ni-Al	B2
In-Tl	FCC	Cu-Zn-Si	B2	U-Nb	BCC(disordered)
Ni-Ti	B2	Cu-Al-Ni	DO3	Ti-Pd-Ni	B2
Cu-Zn-Al	B2, DO3	Ag-Cd		Fe-Mn-Si	FCC(disordered)
Ti-Nb	BCC(disordered)	Cu-Sn	B2		

From Table 2.1, nearly all the alloys have the ordered parent phase. Beside this, as a result of previous discussions;

* The martensitic transformation must involve only a small volume change

* The martensite must be accommodated by twinning, and not involve slip.

2.3. Stress Induced Martensite and Superelasticity

Up to now, it can be carried out that the SME is both thermal and mechanical. Firstly, martensite is initially formed by cooling the specimen to below the M_f temperature, and by applying deformation below the M_f temperature. Then shape recovery occurs by heating the specimen to above A_f temperature. Also, there is another type of shape memory which is independent of temperature: superelasticity [6,21,22].

2.3.1. Stress Induced Martensite

Normally on cooling, the martensite starts to form at M_s under no stress. But in the SMA material, if a stress is applied, then martensite can form above M_s temperature, and the so formed martensite is termed as Stress Induced Martensite (SIM). Here the driving force for the mechanism is not thermal, but mechanical. Figure 2.8 illustrates the proportionality between the required stress to produce SIM and the temperature.

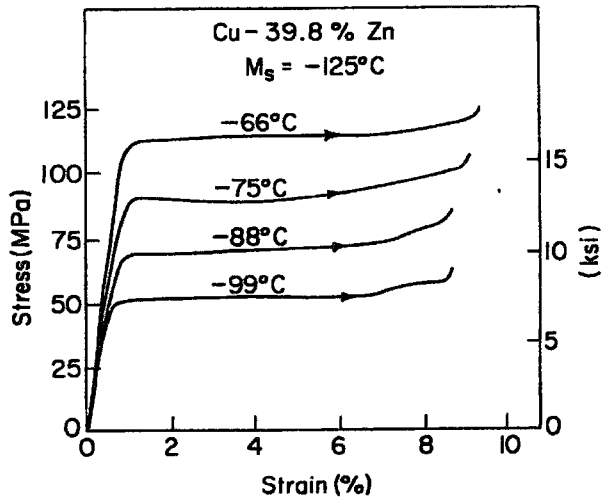

Figure 2.8 Stress-strain curves for a Cu-Zn single crystal loaded in tension above M_s. As the M_s temperature is approached, the stress required to induce martensite is lowered [2].

This increase occurs linearly between stress and the temperature as shown in Figure 2.9 in which the extrapolated stress drops to zero at M_s.

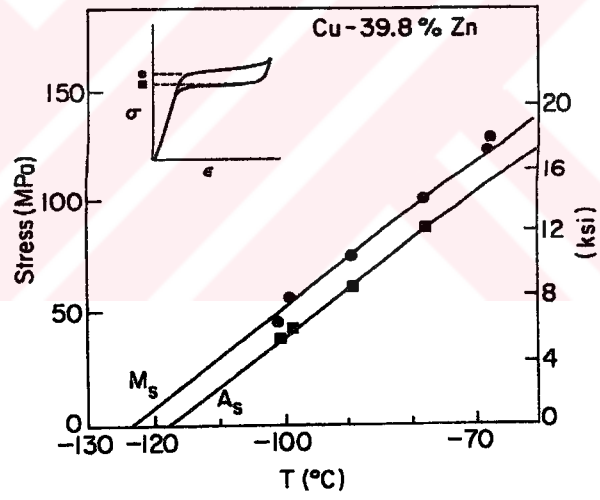

Figure 2.9 The linear plot which obeys the Clasius-Clapeyron equation [2].

The linear variation in stress to induce martensite as a function of temperature obeys the following Clasius-Clapeyron equation [2];

$$dP/dT = \Delta H/T\Delta V \qquad (2.1)$$

where P is the pressure, T is the temperature, ΔH is the transformation latent heat, and ΔV is the transformation volume change. This equation has been traditionally used by chemists, but material scientists use this equation in the form of [2];

$$\sigma/dM_s = -\Delta H/T\varepsilon_o \qquad (2.2)$$

where ΔH and T have the same meanings as before, and σ, M_s and ε_o are the applied stress, the shifted M_s temperature, and the transformational strain resolved along the direction of the applied stress, respectively. But, increasing the temperature with the increasing applied stress is not an unlimited function. Here, after a critical M_d temperature, above which the critical stress to form SIM is greater than that of the needed stress to move dislocations, it is not possible to form SIM. Dominant accommodation process is slip at this level. Therefore, M_d is the highest temperature at which it is possible to have martensite. And the temperature range to form SIM is from M_s to M_d [2].

2.3.2. Superelasticity

Superelasticity is the rubber like behavior of SMAs under certain conditions. Superelasticity occurs when a material is deformed above A_s, but still below M_d. In this range, stability of martensite is obtained by applying or removing the stress. Figure 2.10 shows a "superelastic" stress-strain curve, which can also be described as superelastic loop, for a Cu-39,8%Zn SMA. In the figure, upper region corresponds to the martensite formation under stress and the lower region shows the reversion of SIM when the stress is removed. Another significant feature in Figure 2.10 is that, 9% strain is fully recoverable during unloading, which reveals the mechanical SME [1,2,9].

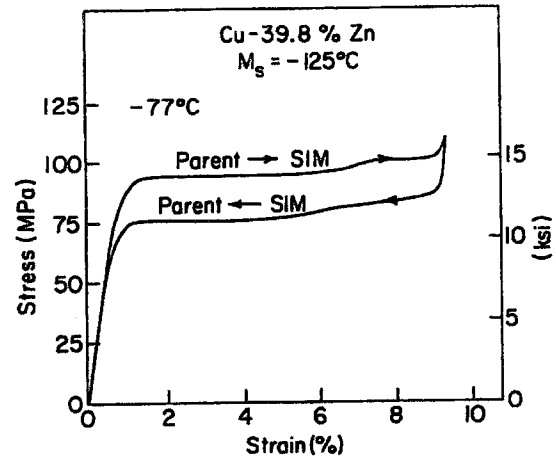

Figure 2.10 Stress-strain curve for a Cu-Zn shape memory alloy loaded above the A_s temperature and then unloaded shows distinct superelastic behavior. SIM is formed during loading, which becomes unstable and disappears upon loading [2].

Figure 2.11 shows a superelastic stress-strain curve for a NiTi SMA spring compared to a conventional spring material, piano wire. The presence of completely

recoverable strain can be seen clearly for the SMA. But, only a one part of strain is recoverable for the piano wire even though they are extended with the same amount.

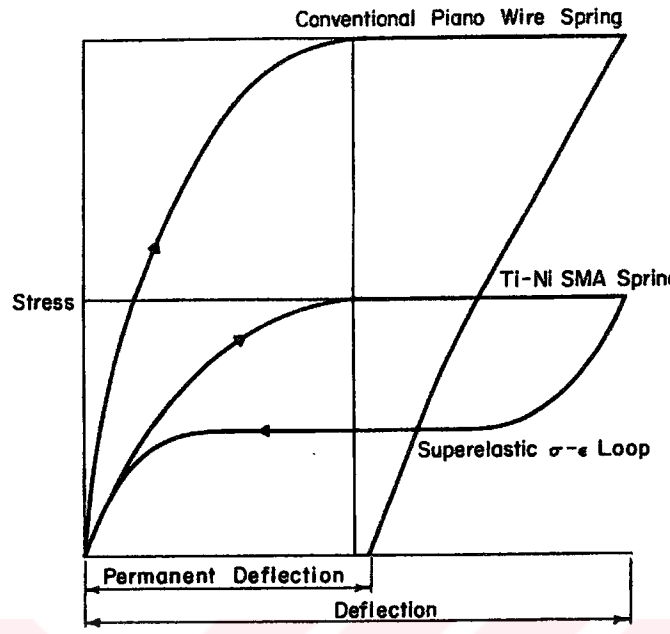

Figure 2.11 Comparison of springs made of superelastic SMA and conventional piano wire [2].

2.4. Two-Way Shape Memory

The ability of SMAs to recover a preset shape upon heating its transformation temperatures and return to an alternate shape upon cooling is known as two-way memory [23]. Two way memory is unique since the material "remembers" different high temperature and low temperature shapes as shown in Figure 2.12. If the figure is looked over, in the upper part, there is a collapsed spring and when it is deformed by extension below M_f, the original spring shape is recovered as the result of the following heating to above A_f. But, when cool the specimen again to below M_f, the original contracted shape remains. This is the one-way shape memory behavior which is a one time only deployment as explained before. On the contrary, in the lower part of the figure, two-way shape memory is seen. In this case, when the original contracted spring extends above A_f and spontaneously contracts again when it is cooled to below M_f. The spring extends again when heated to above A_f and contracts again when cooled to below M_f, repeating indefinitely.

Special thermo-mechanical treatment (training treatments) is required to produce the two-way behavior as shown in Figure 2.13. Although there are several such

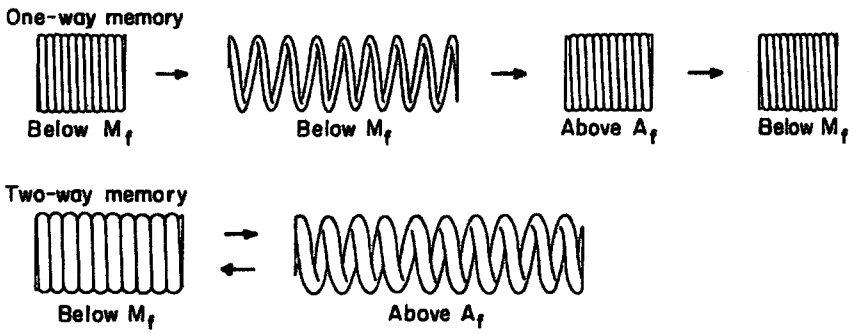

Figure 2.12 Comparison of the one-way (upper) and two-way (lower) shape memories using a coil spring as an example [2].

treatments that can be used, all of them introduce microstresses in the material that lead to bias the nucleation and growth of martensite that can also cause some variants to form preferentially.

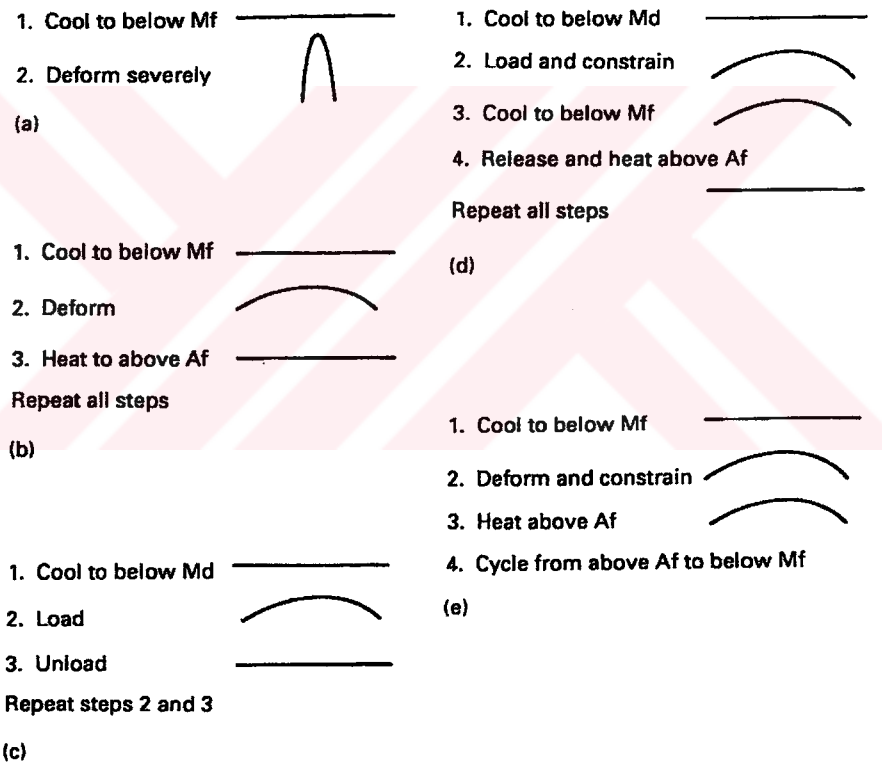

Figure 2.13 Illustration of several training routines that can be used to produce two-way shape memory behavior [24].

There have been more things written about this unique phenomenon in the literature. This has triggered many ideas in the minds of product designers. Some examples of these potential applications include reversible fasteners, temperature sensitive actuators, retrievable medical implants, and toys and novelty items. On the other

hand, there are a number of limitations which should not be connived before attempting to exploit two-way memory behavior as follow;

- The amount of recoverable strain is generally about 2%, which is much lower than that which is achievable in one-way memory (6 to 9%)
- The transformation forces upon cooling are extremely low. The memory can be erased with very slight overheating (as low as 250 °C)
- The long-term fatigue and stability characteristics are not well known [4].

Since SMAs have a unique property in remembering the original shape, have an actuator function and possess superelasticity, they are now being used for various applications such as pipe couplings, various actuators in electric appliance, automobile applications, antenna for cellular phones and medical implants and guide wires etc. Besides, since they have the function of an actuator as well as a sensor, they are promising candidates for miniaturization of actuators such as micro-actuators, micro-machines or robots [3].

3. NiTi BASED SHAPE MEMORY ALLOYS

NiTi is a binary alloy with a near equiatomic composition of Nickel and Titanium. To date, it was found NiTi to be the most suitable SMA in commercial applications. Shape memory properties of NiTi, which led to rapid growth of interest in the shape memory phenomenon, were discovered in the 1960s. The acronym Nitinol or NiTi-NOL is commonly used when referring to Ni-Ti based SMAs since its discovery took place at NOL (Naval Ordinance Laboratory). [2, 25]

3.1. Metallurgy of NiTi Alloys

Ni-Ti SMAs are ordered intermetallic compounds based on the equiatomic composition. From the binary phase diagram (Figure 3.1), melting point of NiTi is about 1310 °C and NiTi has an extended homogeneity around this temperature. This compound is present as the stable phase forming down to room temperature [25]

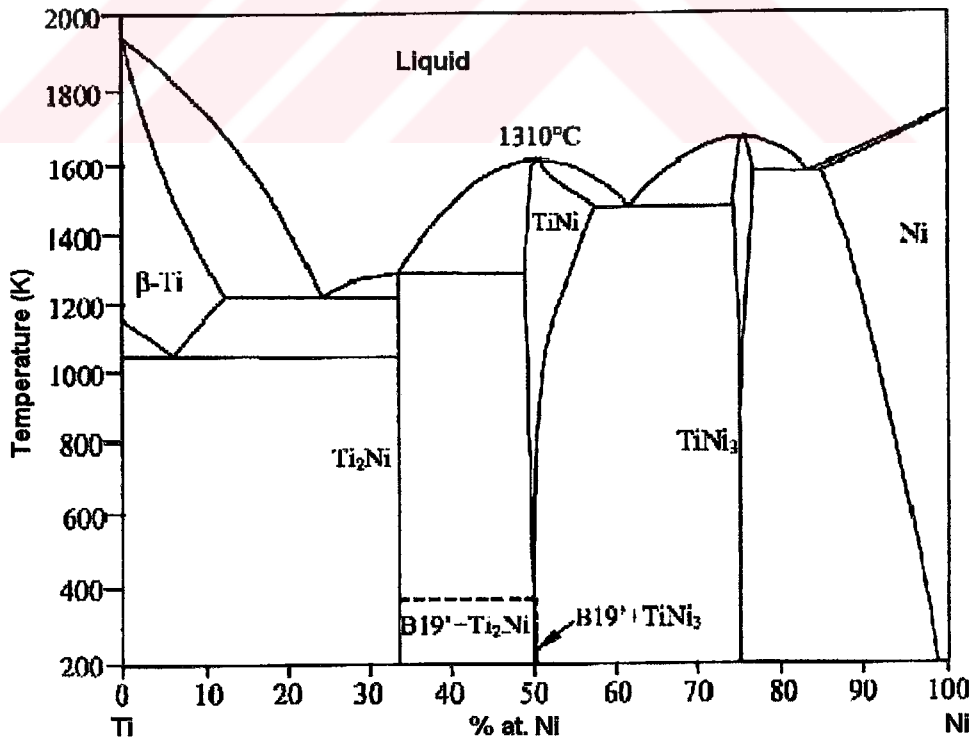

Figure 3.1 Binary Phase diagram of NiTi [26]

The stoichiometric range of NiTi is very narrow at low temperatures and therefore, the alloys usually include precipitates of a second intermetallic phase. Depending on this, microstructure is primarily single phase with small amounts of other phases distributed in the matrix. Titanium is very reactive to oxygen. Thus, oxygen decreases the stoichiometric range of the NiTi compound, and can unexpectedly result in compositions within three phase field such as Ni_x-Ti_y-O_z. For this reason, Ni_3Ti can be present even if the alloy is titanium rich [8]. In addition to these, when the composition of the alloy deviates from stoichiometry, larger precipitates that can affect the hot workability of NiTi will become present especially on the Ti-rich side. Because these large precipitates are brittle, they can often result in cracking.

In the composition range at which the Ni-Ti phase exists at ambient temperature, M_s strongly depends on composition, especially on the Ni-rich side as shown in Figure 3.2. From the figure, it can be carried out that a 1% shift in nickel composition can cause 100 °C change in M_s temperature [27]. This composition dependence of M_s has important practical consequences. In practice, precise composition control is required when melting the alloys.

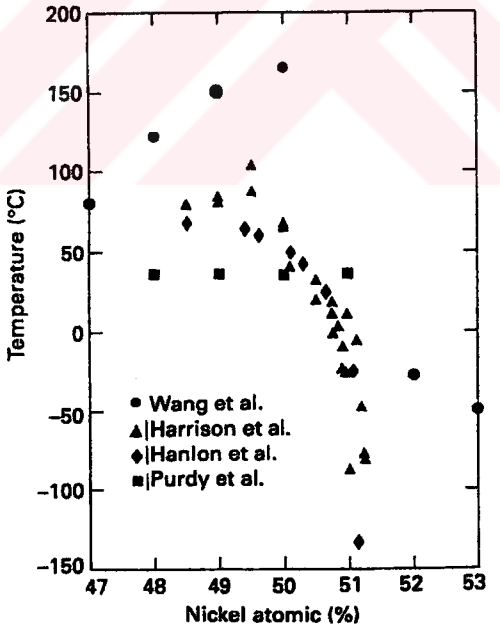

Figure 3.2 The dependence of the transformation temperature M_s on composition [8].

3.2. Crystal Structures and Martensitic Transformations in NiTi

NiTi transforms martensitically from the parent B2 phase (austenite) to a monoclinic B19` phase (martensite) with the best shape memory behavior and pseudo-elasticity results among all the SMAs. Under certain conditions, an intermediate R-phase is also seen between martensitic and austenitic phases. The sensitivity of martensitic transformation almost depends on the fine structure of the parent B2 phase. Therefore, factors such as Ni content, aging, thermo-mechanical treatment and addition of alloying elements, which affect the structure, are also very important for controlling the memory behavior [28, 29]

Near equiatomic NiTi alloys form B2 austenite when cooling down from liquidus temperature (~1573 K) [28]. This phase of NiTi is an ordered CsCl B2 structure meaning that the atoms are situated in specific lattice sites. And the most common martensitic structure in NiTi is also an ordered monoclinic B19` structure. Figure 3.3 shows the crystal structures belonging to parent B2 and martensitic B19` phases. The lattice parameter of the B2 austenite is a_o= 2,99 °A. For the martensitic structure, they are a=2,88 °A, b=4,12 °A, c= 4,62 °A, and β=96,8° [30]. Figure 3.3 also shows the B2 to B19` martensitic phase transformation in NiTi. As it is noticeded, the lattice distortion carries a tetragonal cell of the parent B2 structure into monoclinic cell of the product.

In fully annealed or solution treated near stoichiometric Ni-Ti alloys, when cooling below M_f, as shown in Figure 3.3; B2 phase transforms directly to B19` martensite. However, if thermally cycled or thermo-mechanically treated, they transform in two steps, i.e., from B2 parent to the rhombohedral R-phase, then from R-phase to the B19` phase. B2 to R-phase transformation is also a martensitic transformation. Because the transformation is characterized by a very small temperature hysteresis, and this property makes it useful in thermal actuator applications [9].

3.3. R-Phase Transition

One important field of SMA application is the thermal actuators. Generally, most martensitic transformations are associated with a temperature hysteresis greater than 10 °C. But thermal actuator type devices require small thermal hysteresis. At this point, R-phase transition which is a martensite like transition gain importance with a temperature hysteresis as small as 1,5 °C [31]. The R-phase transition occurs upon

cooling prior to the martensitic transformation in Ni-Ti alloy systems under certain conditions [32].

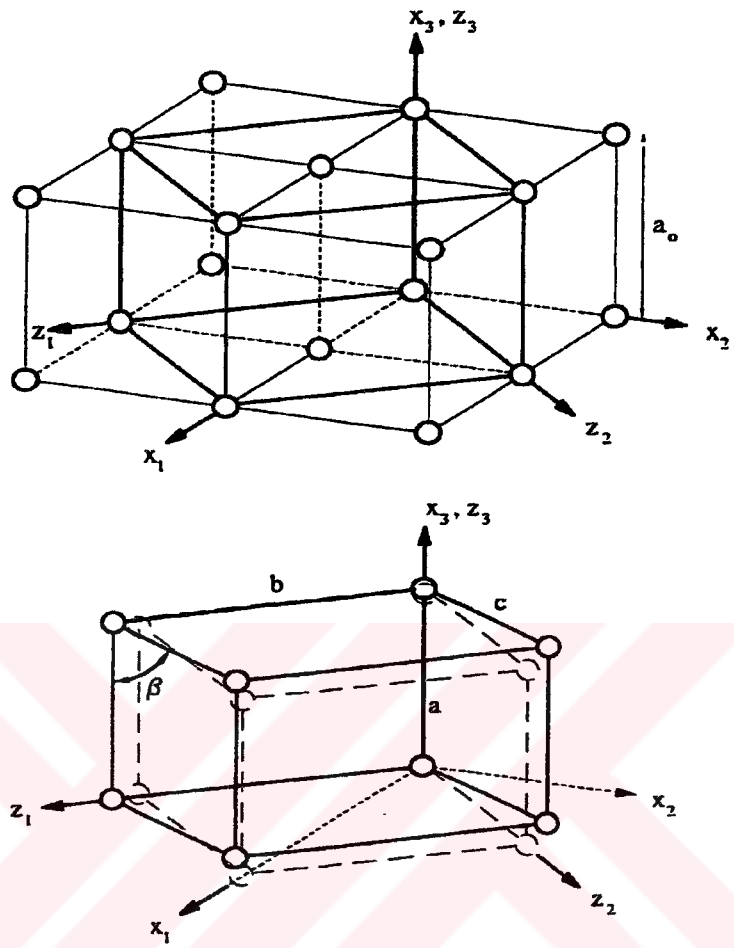

Figure 3.3 B2 to B19` transformation, Top: Crystal structure before the transformation, a tetragonal cell in B2 matrix is delineated. Bottom: the transformed monoclinic cell. Tetragonal cell before the transformation is shown with the dashed line. The axis x_1, x_2, x_3 are along the cube axis, the axis z_1, z_2, z_3 are along the tetragonal axis [9].

In Figure 3.4, it can be observed how lattice changes with decreasing temperature. The parent phase is cubic, and the low temperature phase is rhombohedral, therefore, the transition is called R-Phase transition.

It might be expected to observe shape memory and superelasticity since R-Phase transition is associated with a lattice distortion [33].

The basic approach for realizing the R-phase transition is to recognize the presence of two competing transformations: the R-phase transition and the martensitic transformation. Thus, for the R-phase transition to come into existence, the martensitic transformation relative to the R-phase transition must be suppressed.

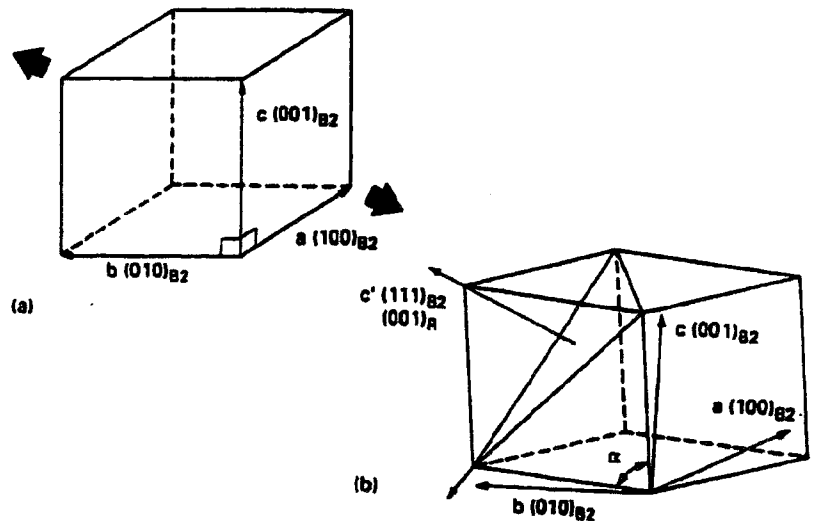

Figure 3.4 Rhombohedral lattice of the R-Phase [9].

There are three ways to do suppress R-phase transition;

- The introduction of rearranged dislocations produced by cold-working then post-annealing at temperatures between 400 and 500 °C
- The introduction of precipitates by solution-treated and aging alloys of greater than 50,5 at.% Ni at temperatures between 400 and 500 °C.
- Addition of certain third elements which enable the suppression of the martensitic transformation

The stability of the SME under cyclic loading conditions is very important when it is used for actuator applications [34]. The R-phase transition was first observed by Dautovich and Purdy, and Wang et. al. [31], but the nature of the transition and the relation with the subsequent martensitic transformation was not clear. Miyazaki and Otsuka made more extensive studies on the associated mechanical behavior, and found superelasticity associated with the transition [31]. They also carried out a quantitative study using single crystals.

Although the recoverable strain is limited to 1 %, the some superiorities of R-phase make it extremely useful for accurate thermal actuators and proportional control devices since the temperature hysteresis is as small as 1,5 °C. Beside these, the temperature – strain curve is quite stable during thermal cycling [31].

3.4. Properties of NiTi Shape Memory Alloys

In Table 3.1, the general properties of NiTi such as transformation temperatures, physical, electrical and magnetic, and mechanical properties are given.

Table 3.1 Selected Properties of NiTi [35].

Transformation Properties	
Transformation Temperature	-200 to 110 °C
Latent Heat of Transformation	5.78 cal/g
Transformation Strain (for polycrystalline material)	for a single cycle.... max 8%
	for 100 cycles.....6%
	for 100,000 cycles.....4%
Hysteresis**	30 to 50 °C
Physical Properties	
Melting Point	1300 °C
Density	6.45 g/cm^3
Thermal Conductivity	austenite.....0.18 W/cm * °C
	martensite.....0.086 W/cm * °C
Coefficient of Thermal Expansion	austenite.....11*10^{-6}/°C
	martensite.....6,610^{-6}/°C
Specific Heat	0.20 cal/g * °C
Corrosion Performance***	Excellent
Electrical and Magnetic Properties	
Resistivity [resistance = resistivity * length / cross-sectional area]	austenite ~ 100 micro-ohms * cm
	martensite.....approx. 80 micro-ohms * cm
Magnetic Permeability	< 1.002
Magnetic Susceptibility	3.0 emu/g
Mechanical Properties	
Young's Modulus****	austenite.....approx. 83 GPa
	martensite.....approx. 28 to 41 GPa
Yield Strength	austenite.....195 to 690 MPa
	martensite..... .....70 to 140 MPa
Ultimate Tensile Strength	fully annealed.....895 MPa
	work hardened.....1900 MPa
Poisson's Ratio	0.33
Elongation at Failure	fully annealed.....25 to 50%
	work hardened..... ....5 to 10%
Hot Workability	quite good
Cold Workability	difficult due to rapid work hardening
Machinability	difficult, abrasive techniques preferred

** Values listed are for a full martensite to austenite transition. Hysteresis can be significantly reduced by partial transformation or ternary alloys.
*** Similar to 300 series stainless steel or titanium
**** Highly nonlinear with temperature

3.5. Measuring Transformation Temperatures

For almost any use of a SMA, it is highly desirable to know the Transformation Temperatures (TTRs) of the alloy, at which the alloy transforms from the higher temperature Austenite to the lower temperature Martensite or vice versa. There are several ways in determining TTRs of SMAs, but three of them are in common use with NiTi alloys to provide helpful data for the designers. These are constant load, DSC, and Active A_f.

Constant loading method is based upon applying a load to the alloy and monitoring its deformation and shape recovery simultaneously as the alloy is cooled and heated through the transformation range as shown in Figure 3.5. Since the TTRs are stress dependent, they will differ under changing loads. Therefore, this state can be used in many actuators by regulating the TTRs with the help of making small adjustments to the bias force acting against the shape memory element. This type of test is generally used for applications which utilize the SME but not the superelasticity in NiTi [36].

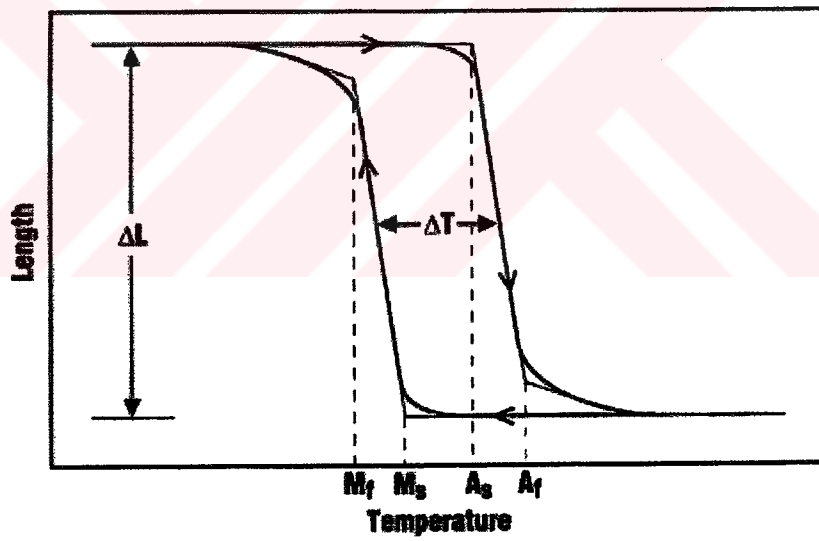

Figure 3.5 Specimen length vs. Temperature in a Constant Load Test of NiTi [36].

DSC is a precise method for determining the TTRs. But it requires an expensive instrument [36]. Figure 3.6 shows the plot that is got from the DSC test. Here, the amount of heat given off or absorbed by a tiny sample of the alloy is measured as it is cooled or heated through its phase transformations. Especially, on fully annealed samples above 700 °C for 10-15 minutes, DSC gives excellent repeatable results [36-39].

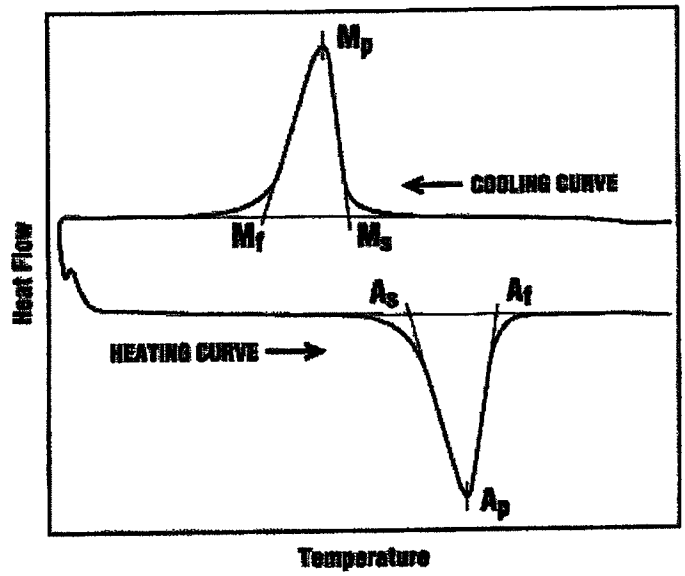

Figure 3.6 A typical DSC curve for a NiTi SMA [36].

The third common method of determining TTRs is known as the Active A_f test. This test is conducted only by bending a sample of the alloy, such as a wire, while it is below M_s. Afterwards, the shape recovery is monitored while the sample is heated and results are plotted as the changing bend angle with respect to the temperature [36].

3.6. Corrosion Behavior of NiTi

Since the discovery of the shape memory properties of nickel-titanium (NiTi) intermetallic in the early 1960s, the alloy has been proposed for various practical applications which did not take its corrosion resistance into account [40-42]. However, for the applications in the human body, the corrosion resistance of NiTi becomes extremely important since the amount and toxicity of corrosion products control the alloy biocompatibility [40].

In the galvanic series, Ni-Ti based alloys are slightly more noble than 316 stainless steel, and show similar corrosion behavior when tested in dilute chloride solutions [8, 40]. When a thin adherent oxide layer known as a passive film is naturally formed, the excellent corrosion resistance is provided. Due to stability of this film, NiTi alloys are resistant to many types of corrosive attacks.

When compared with other commercially available SMAs', NiTi is the most corrosion resistant. For most applications in fields of the actuator, electrical

connectors and fastener, NiTi has a superior corrosion behavior than the other components of the assembly [8].

3.7. Effects of Alloying Elements

When a third element is added to NiTi SMAs, it may have a substantial effect on phase transformation and provide a powerful tool for controlling the properties [8,43]. Addition of the third element such as Cu, Nb, and precious metals can be used to;

- Control the TTRs [14]
- Increase the stability of M_s with respect to thermal history.
- Control the hysteresis width
- Increase the austenitic strength
- Reduce or increase the martensitic strength
- Improve the corrosion resistance
- Suppress the R-phase

The shape recovery temperatures have the highest values at the stoichiometric composition of 50 % at.Ti – 50 % at.Ni in the binary Ti-Ni system. It is about 393 K. It decreases with increasing Ni content and does not change with decreasing Ni content [28].

Ternary alloying additions affect the TTRs. Substitution of V, Cr, Mn or Al for Ti lowers the TTRs. Substitution of Co or Fe for Ni also lowers the martensitic TTRs. Substitution of Fe for Ni separates the TTR ranges of the B2 to R-phase and R phase to B19` transformations effectively. At present, Pd and Au are the only alloying elements, which are known to be effective for increasing the TTRs [28].

3.8. Applications of NiTi Shape Memory Alloys

There are some unique properties of SMAs which make them the perfect choice (and usually the only choice) for many applications. Most commercial applications can be classified in three categories: Superelastic Devices, Shape Memory Actuation Devices, and Martensitic Devices [44].

NiTi superelastic devices are used for applications which demand the extraordinary flexibility and torque ability of NiTi. NiTi has the ability to absorb large amounts of strain energy and release it as the applied strain is removed. Examples of superelastic devices include; medical guide wires, eyeglass frames, cellular telephone antennas, and damping devices etc.

Shape memory actuation devices utilize the shape memory effect to recover a particular shape upon heating above their transformation temperatures. Common actuation temperatures are human body temperature and boiling water temperature. Typical examples are; vascular stents, pipe couplings, electrical connectors, coffeepot thermostats, robotics, and aerospace actuators etc.

The martensitic phase of NiTi has some unique properties which makes it an ideal material for many applications. Firstly, the martensitic phase transformation has excellent damping characteristics due to the energy absorption characteristics of its twinned phase structure. Secondly, the martensitic form of NiTi has significant fatigue resistance and can easily be deformed. Vibration dampers, bendable surgical tools and highly fatigue resistant wires are the examples for martensitic devices [44].

4. THIN FILM OF NiTi SHAPE MEMORY ALLOYS

Thin film NiTi produced by sputtering presents a promising new material for solid state actuation in the MEMS field as well as new opportunities for medical devices. It was in 1990 when sputtering of thin film NiTi began with Walker et al. They were the first group to incorporate thin film NiTi with a micromachining process [13]. They patterned a serpentine spring to the thin film they produced, which contracted when current was applied. Nevertheless, their film was amorphous and was never crystallized.

In 1990, Bush and Johnson at the TiNi Alloy Company showed the first definitive evidence of the SME in NiTi films [15]. Using a single target (50/50 at% NiTi), with a DC magnetron sputtering system they conducted a pre-sputtering step for 3 hours. The as-deposited film was amorphous and after vacuum annealing at 723 K for 30 minutes, the film was crystallized and exhibited the SME even though the TTRs were 100 °C lower than that of the target. Nevertheless, they were the first to think about and to envision NiTi thin film for MEMS application. Since 1990, numerous studies and papers have been published on sputter deposition of NiTi thin film.

Compositional sensitivity of the material on TTRs as shown and explained before (Figure 3.2) is also important if the case is depositing NiTi film with TTRs similar to that of the target [45-47]. A shift of as little as 1 at% can alter TTRs about 100 °C. In addition, Ti is very reactive and can be oxidized due to only small amounts of oxygen contamination inside the system. The binary phase diagram of NiTi (Figure 3.1), shows the complications involved during the heat treatments. The NiTi phase has a very narrow region with numerous possible precipitates at room temperature that have not been documented by any phase diagrams. Thus, if the conditions for crystallization and compositional sensitivity of these materials especially on TTRs are considered, these complications must be taken into account when studying.

NiTi films with TTRs above room temperature are difficult to achieve [48]. In addition to difficulties, deposited films have the one-way SME only. In order to achieve the two-way SME, a biasing force is required to reshape the NiTi when

cooled. Kuribayishi introduced this biasing force by forming different types of precipitates on opposite sides of his films and thus by creating compressive and tensile stresses inside the films [13]. In the martensitic phase the film curled and when it is heated to above A_f, it again flattened. It was because of the higher modulus that overcomes the residual stress. This process requires complicated heat treatments and the stability of these precipitates after numerous thermal cycles are not known. For macroscopic systems, individuals are proposing to combine superelastic elements with shape memory elements to achieve the two-way effect. Therefore it might be advantageous to develop an approach to produce compositionally graded thin films for achieving the two-way effect [13].

4.1. Advantages of Using Thin Film NiTi

The five major advantageous of using thin film NiTi SMA, especially in MEMS field, are (1) potential of large frequency response, (2) large work density, (3) large strain output of SMA, (4) joule heating activation, (5) its biocompatibility [11].

Since NiTi SMAs are heat actuated, improved performance can be achieved at microscales [49]. Specifically, as compared to bulk SMA, for the thin films with a smaller mass and larger surface to volume ratio, heat transfer is substantially increased, power requirements are lowered and large stresses and strains are achievable. All these advantages make NiTi a very promising actuator material for microdevices [50-52]. However, sputtering of NiTi thin film from a 50/50 at% NiTi target produces films with TTRs different from the target due to loss of Ti during sputtering. This fact makes its use as an actuator questionable. Researchers have compensated for this, by placing Ti plates on the target to effectively change the composition of the target or to use a non- equiatomic target.

4.2. Shape Memory Thin Film Processing

Historically the first attempt for thin film deposition was by vacuum evaporation. However, since evaporation rates of Ni and Ti were not the same, this method was unsuccessful to form NiTi thin films with good shape memory properties [9].

Shape memory films can be obtained in different ways such as cold rolling, vacuum plasma spray, ion-sputter deposition, and DC or RF magnetron sputtering. Among them magnetron sputtering is believed to be the simplest and most reliable method to

produce shape memory thin films with desired thickness and composition. Besides, it also has an advantage of batch processing in fabricating microdevices with good adhesion between films and substrates. The major advantages of using magnetron sputtering are as follow;

- Sputtering is an atom-by-atom process. Thus, the obtained films are nonporous (dense) with surfaces which closely reproduce the surface finish of the substrate.
- Greater film thickness and uniformity can be achieved by manipulating the plasma with magnetic fields.
- Large area target which not only improves the uniformity of film thickness, but also makes film thickness control relatively very simple, can be used during magnetron sputtering [10,53,54].

Despite these superiorities of magnetron sputtering, its mechanism is not simple. For example, it is not easy to formulate a theory which would provide the prediction of experimental results without the use of adjustable parameters. In fact, this is because numerous parameters are involved such as kinetic energy of the ions, electronic structure of the collision partners, lattice structure, orientation and binding energy of lattice atoms. Beside these, SMAs are exceptionally sensitive to the alloy's composition. A film's composition is not only affected by the target's composition, but also sensitive to the processing. Therefore, a significant effort has been put forth to understand the effect of the processing parameters such as target power, working distance, substrate temperature, working pressure etc. on the properties of SMA thin films.

4.3. Sputtering Introduction

As a simple definition, sputtering is the ejection of particles by momentum transfer from a target onto a substrate. The entire process is done in a vacuum chamber under typical base pressures of between 10^{-6} and 10^{-10} Torr. Ejection of the target particles is achieved by ion bombardment of the target. A continuous flow of Ar at pressures between 1 to 100 mTorr such that a glow discharge or plasma is established is the most common method of providing ion bombardment. A plasma is an ionized gas with a net charge of zero [10,53].

There is an additional advantage of sputtering process that the deposited film will tend to have the same composition with the target. This is affected by the different sputter yields belonging to various elements in the target. When magnetron sputtering source is used, it improves the sputtering rates between the range of 3 times for RF and 20 to 30 times for DC. The ionization efficiency of the electrons are improved by the magnetic field by allowing a plasma to be sustained at lower Ar pressures (down to a minimum of 0,1 mTorr).

4.4. Sputter Deposited Films of NiTi Alloys

NiTi SMA thin films have been studied during the past years for their potential applications in the field of micro-actuators. Thus, sputter deposition of NiTi alloy thin films is attracting interest as a promising method for producing micro-actuators. Besides, NiTi SMA thin films also enable the development of a new generation sensors. However, there are some difficulties with processing, which have impeded widespread use of the material [28].

Pre-alloyed targets are usually used to obtain thin films of a desired composition. However, films sputter-deposited from the alloy target show Ti depletion and Ni enrichment, most probably due to the difference between the sputter yields (number of atoms ejected for incident ion) of Ni and Ti or oxidation of Ti during the deposition operation. Therefore, the composition is controlled by placing additional pure Ti on top of the target for effectively altering the composition of the target.

As-deposited films are amorphous if the substrate temperature is kept below 473 K and they do not exhibit shape memory. The amorphous films crystallize when they are annealed at a temperature above 673 K [28].

Crystallization occurs by nucleation and growth of B2 phase grains in the amorphous phase. In the coarse of crystallization, no precipitation takes place in near-equiatomic alloy films but Ni_4Ti_3 precipitates in Ni-rich (greater than 50,6 at.%) alloy films. The obtained structures of the near equiatomic and Ni-rich films are compatible with the information obtained for melt-solidified bulk materials. However, the sputter-deposited amorphous films can form much finer B2 phase grains compared to those of the melt-solidified bulk materials depending on the annealing temperature and time.

An electron diffraction pattern from an as-deposited Ni-Ti film is shown in Figure 4.1a. The diffuse rings indicate that the film is amorphous. After annealing the film at 973 K, it crystallizes as it can be seen from the Figure 4.1b. The obtained diffraction pattern corresponds to exhibition of R-phase after crystallization (Figure 4.1c). In each grain, various plates of the R-phase can be noticed. On heating above the R_s (start of R-phase upon cooling), R-phase transforms to B2 parent phase as shown in diffraction pattern in Figure 4.1d and R-phase plates start to disappear. The grain size of B2 phase is 2-3 μm.

Figure 4.1 Electron diffraction patterns of NiTi alloy thin film [28].

There is no essential difference in the shape memory behavior between the sputter deposited crystallized films and the melt-solidified bulk materials as expected from the obtained structures of the films. Furthermore, reduction of the grain size which

can be achieved in the sputter deposited crystallized films, is effective for strengthening the matrix and also for improving the shape memory characteristics. This expression might clarify why the thermo-mechanical approach (cold-rolling and annealing) which is usually applied for bulk materials of near equiatomic composition is not applicable in the case of thin films.

Figure 4.2 shows the elongation-temperature curves obtained by a constant load thermal cycling test on a Ti-51,6at% Ni alloy film. It is obviously seen that the film shows a good SME, which is associated with the two step transformation, on thermal cycling. The SME of sputter-deposited Ni-rich films has also been confirmed by conventional tensile tests.

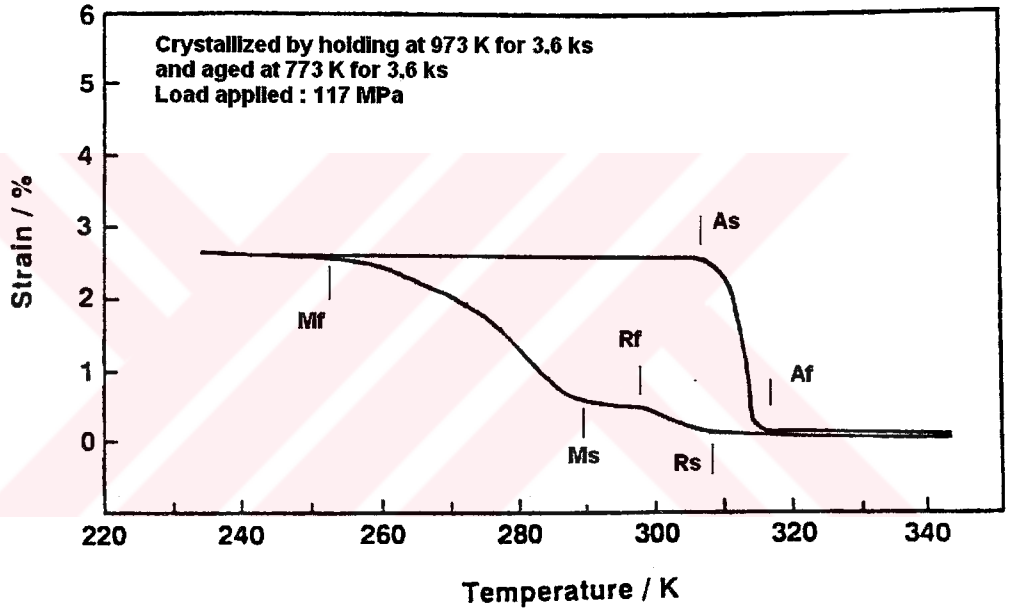

Figure 4.2 Elongation-temperature curve of a sputter deposited Ti-51,6 % Ni alloy film [28].

In contrast to Ni-rich films, Ti-rich films, produced by sputter deposition and crystallization, are quite different in structure and resulting properties from melt-solidified bulk materials.

5. EXPERIMENTAL

The transformation and shape memory characteristics of NiTi thin films strongly depend on metallurgical factors and sputtering conditions. The former includes alloy composition, annealing temperature, aging temperature and time whereas the latter includes Ar pressure, sputtering power (target power), and substrate temperature. The aim of this study was to produce thin films of shape memory NiTi alloy by magnetron sputtering and to investigate their phase transformation behavior with XRD technique. The selected factors to investigate their effects on the crystallization and transformation behavior of NiTi thin films were target power and Ar pressure as the sputtering conditions, and annealing temperature as the metallurgical factor.

As it was observed by many researchers [8, 25-27], generally NiTi thin film compositions show Ti deficiency, when compared to target composition due to lower sputter rate of Ti. In order to overcome this problem, Ti-rich targets or additional Ti targets (multi target system) or near equiatomic Ni-Ti alloy targets were used in the studies. It was also indicated that 1% increase in Ni content in the film composition caused 100 °C decrease in phase transformation temperatures of NiTi alloy [27]. To obtain Ti-rich coatings, Ti-rich alloy target (Ti_{57}-Ni_{43}) was used in this study.

5.1. Substrates

Thin film NiTi alloy coatings were deposited onto high speed steel (HSS) disc substrates with dimensions of 63 x 0,4 mm (diameter x thickness).

5.2. Preparation of Substrates

Standard metallographic techniques were used to prepare the substrates for the coating process. First 9 μm and finally 1 μm diamond paste were used for the polishing of the surfaces of HSS substrates. Substrates were then degreased in C_2HCl_3 (trichloroethylene) solution. After drying the substrates with isopropyl alcohol (IPA), they were immediately placed into the vacuum chamber.

5.3. Thin Film Deposition

NiTi thin films were deposited by a DC magnetron sputtering unit which was mounted in a PVD machine (Model: NVT-12, Novatech-SIE, Moscow). It has an arc PVD cathode and an unbalanced magnetron gun combined with a DC magnetron power supply. Before deposition process, all substrates were pre-heated in front of the arc PVD Molybdenum cathode by applying -600, -800 and -1000 V bias voltages for 2-3 minutes for each.

In this study, a Ti-rich alloy target (Ti- 43%at.Ni) was used in the deposition process. Meanwhile, the target was pre-sputtered before deposition process in order to remove any possible contamination from the target surface.

NiTi thin film system is very sensitive, especially to deposition parameters in terms of shape memory and phase transformation properties. In order to carry out the effects of some parameters and compare them with each other, four different depositions were conducted for this study. The effects of Ar partial pressure and target power on the formation of NiTi thin films were investigated. The rest of the parameters such as target-substrate distance, deposition time, and ambient temperature were kept constant to eliminate their effects on the properties mentioned above. The experiments were conducted under different Ar pressures (2 and 7,5 mTorr) and target powers (300 and 500 W) (Table 5.1).

Table 5.1 Conditions for the deposition of NiTi thin films.

Sample Code / Parameters	KTF638	KTF639	KTF640	KTF641
P_{Ar} (mTorr)	2	2	7,5	7,5
Target Power (W)	300	500	300	500
Ar Flow Rate (sccm)	58	56	58	54
Time (min.)	40	40	40	40
Target-Substrate Distance (cm)	6	6	6	6

5.4. Compositional Analyses

The compositions of the NiTi thin films were determined with a Noran Instruments Voyager VGR II EDS unit connected to a Jeol JSM-6400 SEM. The results were obtained under accelerating voltage of 15 kV and 200X magnification.

5.5. Heat Treatment (Post-annealing)

Formation of as-deposited thin films ends with an amorphous structure when the deposition temperature is kept below 473 K. The amorphous films crystallize when they are annealed at a temperature above 673 K [28]. But, in order to prevent the oxidation of titanium in the film, post-annealing must be performed under high vacuum. For this purpose, samples were annealed at three different temperatures of 550, 700 and 775 °C under high vacuum. Post-annealing of films was conducted with TCU 2000/20 Temperature Control Unit of Philips X'Pert Pro model XRD. Annealing of the films was performed by placing the coatings on a platinum sheet to which a thermocouple was welded. The platinum sheet has the ability to be heated to 1600-1700 °C. The applied vacuum values were in the range of 10^{-3}-10^{-4} mTorr (Table 5.2). Thus, the effect of annealing temperature on the crystallization and phase transformation of NiTi thin films were investigated. Annealing time was 30 minutes.

Table 5.2 Annealing conditions for the as-deposited NiTi thin films.

Sample	Annealing Temperature (°C)	Pressure (mTorr)	Time (min.)
KTF638	550	$5{,}6 \cdot 10^{-4}$	30
300 W	700	$3{,}7 \cdot 10^{-4}$	
2 mTorr	775	$7{,}5 \cdot 10^{-4}$	
KTF639	550	$5{,}6 \cdot 10^{-4}$	
500 W	700	$3{,}7 \cdot 10^{-4}$	
2 mTorr	775	$7{,}5 \cdot 10^{-4}$	
KTF640	550	$5{,}4 \cdot 10^{-4}$	
300 W	700	$3{,}9 \cdot 10^{-4}$	
7,5 mTorr	775	$6{,}0 \cdot 10^{-4}$	
KTF641	550	$5{,}4 \cdot 10^{-4}$	
500 W	700	$3{,}9 \cdot 10^{-4}$	
7,5 mTorr	775	$6{,}0 \cdot 10^{-4}$	

5.6. X-Ray Diffraction Analyses

5.6.1. Phase Analyses

The crystal structures and phases of as-deposited and annealed samples were determined by X-ray Diffraction (XRD) method with Philips PW 3710 X'Pert CuK_{α} diffractometer including ICDD database. The XRD unit has the ability to perform thin film characterization with its thin film attachment. All XRD experiments were conducted under the same conditions (Table 5.3).

Table 5.3 The conditions for the XRD experiments.

Sample Code	T_{anneal} (°C)	V(kV)	I (mA)	W (incident X-ray angle)	2θ	Step size
KTF638	550	40	40	2 °	30°-80°	0,02 °/s
	700					
	775					
KTF639	550					
	700					
	775					
KTF640	550					
	700					
	775					
KTF641	550					
	700					
	775					

5.6.2. Transformation Experiments

Since shape memory materials involves phase transformations, it is usually necessary to do transformation experiments with XRD during heating or cooling the samples. For heating and cooling of the samples, a chiller made up of copper block in which a mixture of water and anti-freeze flows was used. By performing these experiments, it was expected to observe the formation of cubic austenite phase during heating. Here, the upper limit in this system was about 80 °C and therefore, the transformation experiments were conducted at 70-75 °C for all of the samples.

5.7. Structural Analyses

5.7.1. Hardness Measurement

Hardness of the films were measured by a Fischerscope H 100 XYPROG dynamic ultra microhardness tester equipped with an elongated Vickers type indenter. The defined load is applied to the sample with pre-defined loading step number and time intervals. In order to measure hardness inherent to the coating, the indenter should not penetrate to depth more than 1/7 – 1/10 of the total coating thickness. 35 mN load was applied to as-deposited and annealed coatings for hardness measurement. Step number of loading was 120 with 0,5 s pausing time between steps. Each measurement was repeated at least 15 times to obtain an average hardness value.

5.7.2. Thickness Measurement with XRF

The XRF test method has evolved as one of the most widely used non-destructive test methods for coating thickness measurement due to its precision and versatility. In this method, characteristic x-rays from substrate, thin film and if it is present from the interlayer are detected. These energies are distinguished according to their intensities and recorded as the electrical signals, and thickness is measured with the change in the intensity of a particular x-ray radiation. Generally two basic measurement methods are present. The former is based on emission principal that is related with x-rays generated by the thin film, and latter is based on absorption and transmission methods related with the interaction coming from the substrate (x-rays generated by the substrate). In this study, a Fischerscope XDL X-ray System working with emission principal based on x-rays generated by the film was used to measure the film thickness.

5.7.3. Cross-section SEM Analyses

In order to investigate the thickness and the cross section morphology of the films, Jeol JSM-5410 Scanning Electron Microscope was used. The cross-sectional morphologies of the amorphous and crystallized structures annealed at different temperatures were visualized. The thickness of the films were determined from the cross-sectional micrographs using the Semafore 3.01 software. The results were compared with the ones obtained by XRF.

6. RESULTS AND DISCUSSION

6.1. Compositional Analyses

The nominal composition of the target used in this study was $Ni_{43}Ti_{57}$ (atomic ratio). The compositions of the NiTi thin films were examined by SEM/EDS as listed in Table 6.1.

Table 6.1 The results of compositional analyses belonging to deposited films

Sample	Atomic %		Ti : Ni
	Ni	Ti	
Target	43,0	57,0	1,33
KTF638 (300 W- 2 mTorr)	45,0	55,0	1,22
KTF639 (500 W- 2 mTorr)	43,1	56,9	1,32
KTF640 (300 W- 7,5 mTorr)	41,9	58,1	1,38
KTF641 (500 W- 7,5 mTorr)	41,3	58,7	1,42

Since transformation temperatures of NiTi-based SMA films are very sensitive to the composition of the films, the accuracy of compositional analyses gains importance.

As Ho et al. [15] reported that depending on lower sputter rate of Ti, and high reactivity of Ti to oxygen and ability to be oxidized due to only small amounts of oxygen contamination inside the system, the films showed Ti depletion compositionally, meaning that lower Ti content when compared to target at the end of the deposition process. Moreover, as mentioned before (3.1 and 4), a 1% increase in Ni composition may cause 100°C decrease in phase TTRs of a NiTi alloy [27]. In order to prevent Ti depletion and obtain films having TTRs around room temperature, researchers used near-equiatomic targets supplied with separate Ti target (multi-target system) in their coating processes [15].

But, although a Ti-rich target (Ti_{57}-Ni_{43}) was used in our study, only two of the films showed Ti deficiency when compared to target composition as seen in Table 6.1, meaning that coating parameters, especially target power and Ar pressure have important roles on film composition. The results showed that increase in Ar pressure showed higher Ti content in the film. The highest Ti content was obtained for KTF641 coded NiTi film. And the highest TTRs were determined qualitatively for

the KTF641 film annealed at 775 °C when XRD patterns observed in the following parts. Shortly, increase in Ar pressure and target power resulted with increase in Ti content of the film.

6.2. Phase Analyses

Crystal structures belonging to as-deposited films and films annealed at different temperatures under high vacuum were determined by XRD method. The films were not peeled off from the substrate indicating a good adhesion of the films to substrates.

The XRD experiments of as-deposited films revealed clearly that all as-deposited films were in amorphous state. In fact, Fu et al. [55] reported that substrate heating (between 573- 723 K) before deposition tended to obtain films in crystalline form achieving good SME without any need for post-annealing. But in our study, although all substrates were pre-heated in front of the arc PVD cathode by applying different bias voltages for a while as mentioned in part 5.3, it couldn't be managed to observe the effect of substrate heating as Fu reported. However, it is a fact that magnetron sputtering does not exhibit a significant heating effect on the substrates.

The as-coated amorphous films were annealed under vacuum and the annealed structures and their phase transformations were investigated by XRD during heating to 70 °C. Thus, when analyzing XRD patterns after annealing, the patterns obtained from transformation experiments were also taken into account in order to define the phases correctly by controlling appearing or increasing intensity of B2 –austenite peaks and disappearing or decreasing intensity of B19`-martensite peaks during heating. After heat treatment, due to the color alteration on the surfaces of the deposited films, it was obvious that there were very thin oxide layers on the film surfaces although the films were annealed under high vacuum conditions. But XRD patterns did not involve any peaks corresponding to oxide phases. Therefore, the formed oxides during annealing can be defined to be very thin and in amorphous state. Because oxide layers were not met in the XRD patterns, the analyzed phases were determined from the alternatives of NiTi (in austenitic and martensitic forms) as the matrix phase and Ti_2Ni, Ni_3Ti and Ni_4Ti_3 precipitates as the second phases. The most intensive peaks belonging to aforementioned phases were between 2θ =39-45° (see Appendix B).

6.2.1. KTF 638 NiTi film (300 W- 2 mTorr)

For KTF638 coded NiTi films, although as-deposited film was amorphous, annealing this film at 550 °C was not adequate to crystallize this film (Figure 6.1). From the figure, it can also be seen that increasing annealing temperature to 700 °C resulted in the crystallization of the precipitates. The major phases in 700 °C annealed KTF638 NiTi film were Ti_2Ni, Ni_3Ti and Ni_4Ti_3 second phase precipitates. As it is seen in Figure A.1, because no significant difference was detected in transformation experiment of 700 °C annealed film, neither austenitic nor martensitic phases were met in the XRD pattern of the 700 °C annealed film.

For the 775°C annealed KTF638 coded NiTi films, XRD patterns involved the NiTi phases beside the precipitates of second phases. Here, there was a little difference in the transformation experiment patterns conducted at 70 °C. The increase in the intensity of distinctive peaks belonging to B2 – austenitic phase at $2\theta = 61{,}98^{\circ}$ and $78{,}15^{\circ}$ which correspond to (200) and (211) planes respectively, showed the presence of austenitic phase in the film (Figure A.1).

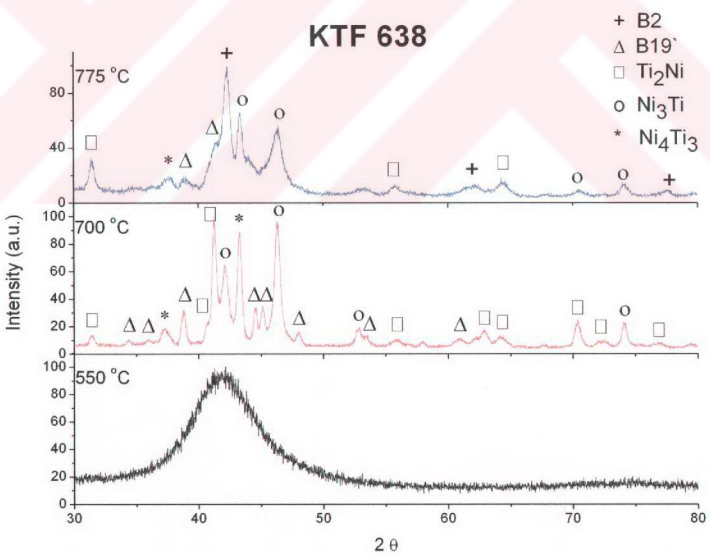

Figure 6.1 XRD patterns obtained for KTF 638 films produced at 300 W- 2 mTorr P_{Ar} and annealed at different temperatures.

For KTF 638 coded films, after the crystallization, the majority of the peaks obtained from XRD patterns belonged to the precipitates. Even though the film was Ti-rich, presence of Ni_3Ti and Ni_4Ti_3 precipitates was also a striking result.

The possible reasons for this observation were mentioned in part 3.1. Yang et al. reported the formation of the precipitates as follows; because of the existence of many vacancies and other defects in the films, and also the very small grain size and large number of grain boundaries after crystallization, it was easier for atoms to diffuse and the precipitation process was faster. They also confirmed this result by calculating the diffusion activation energies and found that the activation energies of formation of precipitated second phases are smaller than that of the formation of B2 and B19` phases [56].

6.2.2. KTF 639 NiTi film (500 W- 2 mTorr)

KTF639 coded as-deposited films were amorphous. Films were annealed at 550, 700 and 775 °C under high vacuum. XRD patterns obtained from the film annealed at 550 °C showed B2 peaks as the major phase and B19` peaks with low intensities (Figure 6.2). Beside these, there were some weak peaks belonging to Ti_2Ni precipitate. Here, while analyzing the patterns, again the patterns obtained from transformation experiment were utilized (Figure A.2). When the film was heated to 70 °C and thereafter XRD experiment conducted, the intensity of the peaks belonging to B2 austenite phase at $2\theta = 42{,}9^{o}$, $61{,}9^{o}$ and $78{,}1^{o}$ which were corresponding to (110), (200) and (211) planes respectively, increased.

When crystallization behavior of 700 °C annealed film is examined from Figure 6.2, again by taking its transformation experiment (Figure A.2) into account during phase analyses, the major phases met in XRD patterns were belonging to second phase precipitates of Ti_2Ni and Ni_3Ti, which is similar with 700 °C annealed KTF 638 NiTi film. However, XRD patterns also involved peaks of B2 and a little amount of B19` peaks.

XRD patterns of the films annealed at 775 °C were also determined. The crystallization results were similar to the ones annealed at 550 °C meaning that the majority of the peaks were B2 austenite phase whereas there were little amount of B19` martensite and Ti_2Ni precipitate phases. XRD patterns obtained from

transformation experiments as shown in Figure A.2 were evaluated while determining the phases.

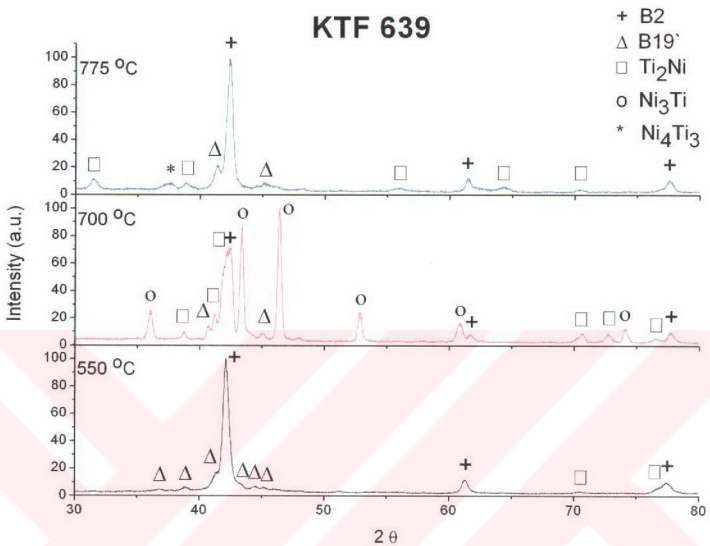

Figure 6.2 XRD patterns obtained for KTF 639 films produced at 500 W- 2 mTorr P_{Ar} and annealed at different temperatures.

As a summary of KTF639 coded films, the XRD patterns obtained from the films annealed at 550 °C and 775 °C showed similarities with each other. However, patterns for the ones, annealed at 700 °C, involved precipitated second phases as the major phases, which revealed that there is a temperature range appropriate for the formation of second phase precipitates. Miyazaki et al. [57] studied on the evaluation of the internal structure as a function of heat-treatment temperature and defined this temperature range as the intermediate temperatures at which a mixture of Ti-rich plate precipitates and equilibrium Ti_2Ni precipitates form. Our study showed this temperature range around 700 °C.

6.2.3. KTF 640 NiTi film (300 W- 7,5 mTorr)

XRD patterns of KTF640 coded NiTi films showed significant differences depending on annealing temperatures. XRD results of 550 °C annealed films were similar to the ones obtained from KTF638 NiTi film annealed at 550 °C. But, KTF638 NiTi film

annealed at 550 °C was in amorphous state. However, from Figure 6.3, KTF640 coded film annealed at 550 °C crystallized partially. Since the width of the peaks gave information about the grain size of the films, obtained peaks from the film can be determined as wide peaks belonging to B2 austenite phase meaning that the grains were fine or crystallization has already started to take place. When observed, among the phases and the crystallization sequence of the phases, B2 was the first phase crystallized through transition from amorphous to crystalline form. The peaks at 2θ = 42,9°, 61,9° and 78,1° which were corresponding to (110), (200) and (211) planes of B2 austenite phase, respectively, were the indicator of the crystallization of B2 phase.

For the film annealed at 700 °C, the obtained XRD patterns showed all of the peaks belonged to second phase precipitates of Ti_2Ni and Ni_3Ti (Figure A.3). Finally, XRD patterns for the film annealed at 775 °C included phases of B2 austenite and Ti_2Ni precipitate as shown in Figure 6.3. Patterns obtained from transformation experiment also verified this evaluation (Figure A.3).

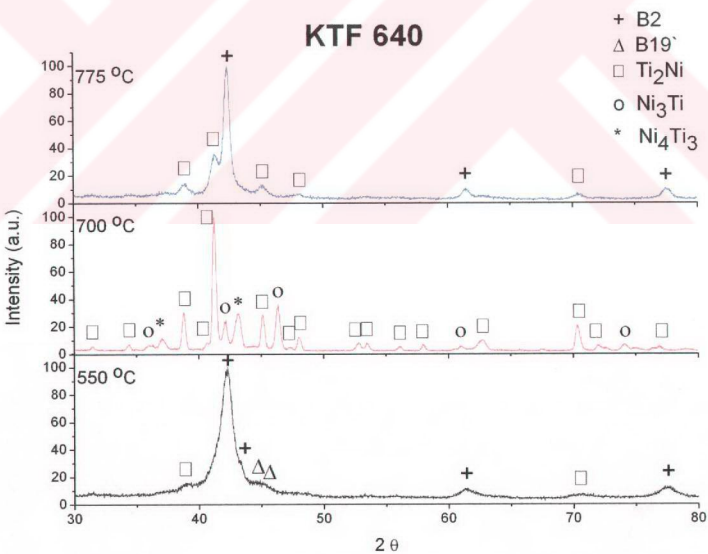

Figure 6.3 XRD patterns obtained for KTF 640 films produced at 300 W- 7,5 mTorr P_{Ar} and annealed at different temperatures.

As the results for KTF 640 NiTi films annealed at 550, 700 and 775 °C, annealing at 700 °C formed second phase precipitates which were similar with the films of KTF638 and KTF639 annealed at 700 °C. And the patterns obtained for the film annealed at 775 °C showed similarity with the KTF639 coded film annealed at 775 °C.

6.2.4. KTF 641 NiTi film (500 W- 7,5 mTorr)

The most striking results were obtained for KTF 641 NiTi films. When XRD patterns were examined step by step with respect to increasing annealing temperature; it can be carried out that, with increasing annealing temperature, crystallizations of the films were completed with involving the martensitic B19` phase as the major phase (Figure 6.4) which can also be followed from Figure A.4. For the film annealed at 550 °C, the dominant phases belonged to austenitic B2 phase. When the annealing temperature was increased to 700 °C, the difference between the intensities of martensitic and austenitic peaks started to decrease, meaning that formation of martensite was started to be preferred to austenite with increasing temperature. And

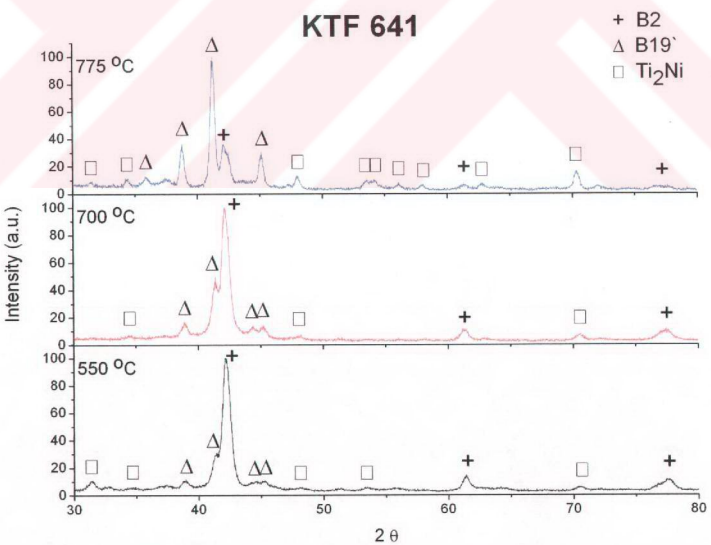

Figure 6.4 XRD patterns obtained for KTF 641 films produced at 500 W- 7,5 mTorr P_{Ar} and annealed at different temperatures.

finally, for the films annealed at 775 °C, the structure exhibited martensitic B19` phase as the major phase. Transformation experiments of this film verified the results above (Figure A.4). If the intensities of the peaks at $2\theta = 41{,}3^{o}$ for martensite and at $2\theta = 42{,}9^{o}$ for austenite which corresponded to (1-11) and (110) planes, respectively, were followed, the result can be noticed clearly. Also when an additional XRD experiment was performed after 70 °C transformation experiment, the patterns matched with the ones obtained as-annealed film, which showed reversibility and repeatibility of the phase transformation between martensitic B19` and austenitic B2 phases.

These results showed that TTRs of films increased with increasing annealing temperature. Surbled et al. obtained similar results while working on compositionally different types of films [45].

As an overall summary for the phase analyses, the most desirable results were obtained from KTF641 NiTi films. The effect of the annealing temperature on the crystallization behavior of the films can be seen obviously. The films except this one exhibited mixed type crystallization for which the crystallization behavior results depending on the annealing temperature can not be generalized. Especially annealing at 700 °C crystallized the films showing completely second phase precipitates.

6.2.5. Shifts in the Position of Peaks

When compared with the standard positions of the peaks (Appendix B), obtained XRD patterns revealed significant shifts in peak positions occurred as the result of residual stress present in the structure of the films (Figure 6.5). When observed in detail (Figure A.5), shifts were tended to occur to the left side of the standard positions which gives an idea whether the stress is in tensile or in compressive form. However, coatings usually involve or expected to involve compressive stress.

Virtually, all deposited films are in stressed condition including thermal, intrinsic and transformational stresses. Thermal stress is originated from the difference in the coefficient of thermal expansion between NiTi films and the substrate. The intrinsic stress critically depends on mismatch between film and substrate, deposition rate, substrate temperature, working gas pressure, and impurities level, etc. Transformational stress is related to the transformation characteristics. Stresses not

only affect transformation behavior and lifetime of fabricated devices, but also can cause the deformation of the deposited films, even fracture [58]. Thus, it is also important to investigate the stress in the deposited NiTi film in order to optimize and control its performance, which can be evaluated as an individual study.

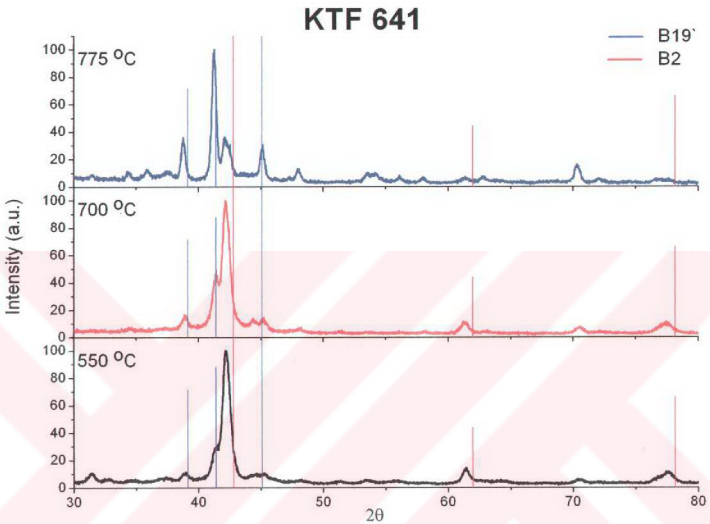

Figure 6.5 Shifts in peak positions of KTF641 films produced at 500 W- 7,5 mTorr P_{Ar}.

6.2.6. Effect of Annealing Temperature on Crystallization and Transformation of the Films

In order to evaluate the effect of changed coating parameters on the crystallization behavior of the films, the XRD patterns for each annealing temperature of each coating were examined (Figures 6.6 – 6.8).

For annealing at 550 °C, XRD patterns of KTF638 film with 300 W target power and 2 mTorr Ar partial pressure showed no crystallization that the film was still in amorphous state (Figure 6.6). For the one with the same target power but increased Ar partial pressure (KTF 640) showed crystallization which has already started that the peaks were too wide that the structure involved fine grains. On the contrary, coatings deposited at 500 W target power showed more uniform crystallization. However, XRD patterns involved B2 austenitic phase as the major phase.

Due to sharpness and intensity of the peaks, for the films annealed at 550 °C, effect of target power on film crystallization is more significant than Ar partial pressure.

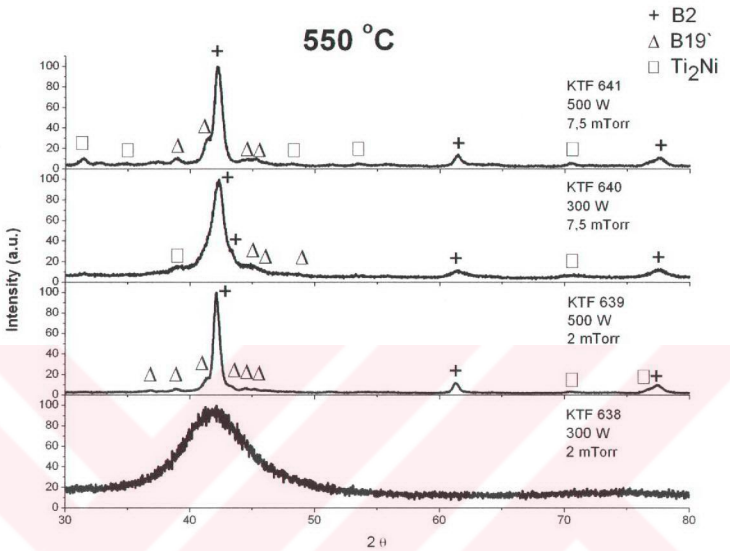

Figure 6.6 The crystallization behaviors of the films deposited under different conditions and annealed at 550 °C.

The films produced at lower target powers, crystallization was not uniform and the peaks were too wide showing very fine grains that crystallization has already started.

Annealing at 700 °C showed similar crystallization behavior for the films except KTF641 deposited at 500 W target power and 7,5 mTorr partial pressure of Ar (Figure 6.7). In the XRD patterns of the films, precipitated second phases were present with small orientation differences. Unlike these films, KTF641 film exhibited the B2 austenite (as the major phase) and B19` martensite phases in XRD patterns.

For 700 °C annealed films, the ones produced at lower target power showed similar crystallization behavior whereas the others produced at higher target power showed different crystallization behavior. At this point, at high target power, increasing Ar partial pressure tended to form B2 austenitic phase with a small amount of B19` martensitic phase. As a result, when wanted to prevent or minimize precipitate

formation, 700 °C annealing is an appropriate annealing temperature just for the film produced at 500 W- 7,5 mTorr Ar pressure.

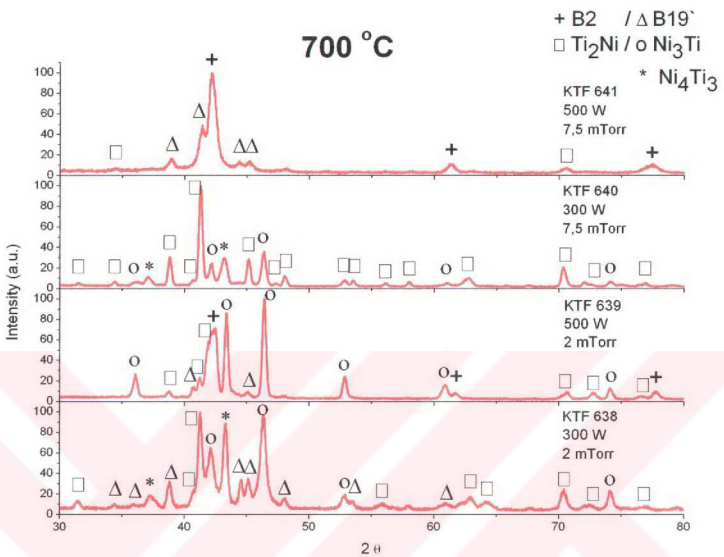

Figure 6.7 The crystallization behaviors of the films deposited under different conditions and annealed at 700 °C.

For the crystallization behaviors of the films annealed at 775 °C, the significant difference can be seen in KTF641 with mixed phase structure of B19` martensite (as the major phase) and B2 austenite. KTF639 and KTF640 films showed very similar crystallization behavior containing B2 austenite as the major phase and B19` martensitic phase whereas second phase precipitates (Ni_3Ti as the major phase) were dominant phases for KTF638 film as shown in Figure 6.8. In order to obtain films with TTRs around room temperature with minimum second phase precipitate formation among four different deposition processes, the deposition conditions of KTF641 NiTi film seemed to be the ideal ones.

For 775 °C annealed films, the one produced at low target power – low argon partial pressure showed mixed patterns including second phase precipitates. Increasing target power and Ar partial pressure for 775 °C annealed films showed B19`

martensitic phase as the major phase in the patterns indicating that TTRs increased, which was also reported by Surbled et al. [45] in their study.

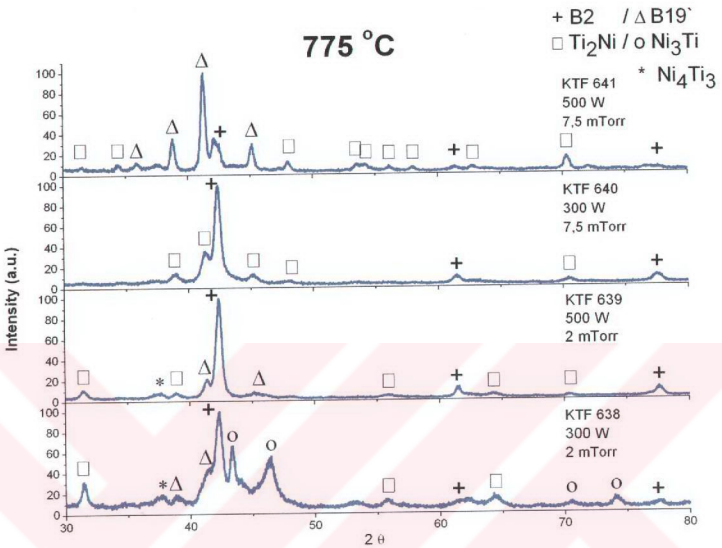

Figure 6.8 The crystallization behaviors of the films deposited under different conditions and annealed at 775 °C.

As the result of effect of the different annealing temperatures, the film produced at 300 W- 2 mTorr showed an amorphous structure when annealed at 550 °C. Annealing at 700 °C showed formation of second phase precipitates (Ti_2Ni, Ni_3Ti and Ni_4Ti_3) as the major phases. Annealing at 775 °C also resulted with the crystallization of precipitate phases.

Annealing of the films produced at 500 W- 2 mTorr resulted with the crystallization of second phase precipitates for 700 °C, whereas XRD patterns for 550 and 775 °C annealing showed similar crystallization behavior which was the formation of B2 austenitic phase as the major phase and B19` martensitic phase and Ti_2Ni precipitates as the minor phases.

For the films produced at 300 W- 7,5 mTorr, annealing at 550 and 775 °C showed the crystallization of B2 austenitic phase as the major phase. Formation of Ti_2Ni was noticed near austenitic phase for 550 °C annealing whereas B19` martensitic phase

was also found as the minor phase beside Ti_2Ni precipitate for 775 °C annealing. 700 °C annealing resulted with the crystallization of second phase precipitates Ti_2Ni was the major phase for 700 °C annealing.

Films produced at 500 W- 7,5 mTorr resulted with the crystallization of B2, B19` and $Ti_2Ni$ precipitate phases with varying majorities between B2 and B19`. 550 °C annealed film showed B2 austenitic phase as the major phase whereas 775 °C annealing resulted with the crystallization of B19` martensite as the major phase.

As a result, films annealed at 700 °C generally resulted with the crystallization of second phase precipitates as the major phases. Annealing at 550 and 775 °C showed sometimes similarity in terms of the formation of B2 austenite as the major phase. Also, especially for the films produced at 500 W- 7,5 mTorr, increasing annealing temperature increased TTRs of the film qualitatively due to the presence B19` martensite as the major phase at room temperature.

6.2.7. Effect of Coating Parameters on Crystallization and Transformation of the Films

550 °C annealing of the films produced at different target power and argon partial pressures showed nearly similar crystallization behaviors whereas the one produced at 300 W- 2 mTorr resulted with amorphous structure. Films produced at 500 W, showed more significant crystallization than the films produced at 300 W due to the sharpness of the peaks indicating the fine grains. Effect of P_{Ar} can be noticed at transition from amorphous to crystalline structure for the films produced at 2 and 7,5 mTorr.

When observed 700 °C annealing of the films produced at different target power and Ar partial pressure, all the films resulted with the crystallization of the second phase precipitates except the one produced at 500 W- 7,5 mTorr. This film showed formation of B2 austenite as the major phase and B19` martensite as the minor phase. P_{Ar} was effective on the formation of second phase precipitates. While the films produced at 2 mTorr showed Ni_3Ti precipitate as the major phase, the film produced at 7,5 mTorr resulted with the crystallization of Ti_2Ni precipitate as the major phase.

775 °C annealing of the films produced at different target power and argon partial pressure showed strong dependency to the coating parameters in terms of the formations of B2 austenitic and B19` martensitic phases. Especially for the two

produced at 7,5 mTorr, increasing target power resulted with the crystallization of B19` as the major phase indicating the increased TTRs of the film. The film produced at 300 W- 2 mTorr showed crystallization of second phase precipitates near B2 austenitic phase. Meanwhile, the similarities between the obtained results from the films produced at 500 W- 2 mTorr and 300 W- 7,5 mTorr can be noticed as an interesting point.

6.3. Structural Analyses

6.3.1. Hardness Measurement

The hardness of as-deposited and annealed films were measured with ultra microhardness tester (Table 6.2). Depending on the phase analyses results, hardness of the films changed in a wide range as shown in Figure 6.9.

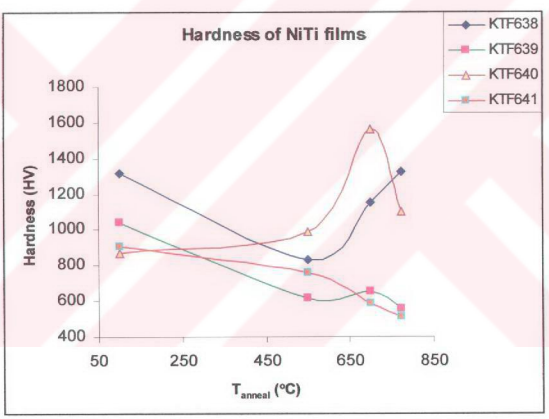

Figure 6.9 Hardness of the films for as-deposited states and annealed at different temperatures.

As a general evaluation, the hardness of the as-deposited films decreased with increasing Ti content. Due to the formation of second phase precipitates after annealing at 700 °C, there occurred a significant increase in the hardness of the films. In addition, generally the deformation is usually applied to NiTi SMA when the structure is in martensitic phase due to its mechanical properties (Table 3.1). KTF641 film showed a decrease in hardness with the formation of martensitic phase at higher annealing temperatures. It can also be seen that that the elastic stiffness became

weaker with decreasing value of Young Modulus with increasing annealing temperature (Table 6.2).

Table 6.2 The hardness measurement results of the films.

Samples	T_{anneal} (°C)	Hardness (HV)	$E/(1-\upsilon^2)$ (GPa)	Present Phases (from major to minor)
KTF638 300 W 2 mTorr	As-deposited	1313 ± 15	190 ± 1	Amorphous
	550	834 ± 30	168 ± 2	Amorphous
	700	1153 ± 19	158 ± 3	Ni_3Ti, Ti_2Ni, B19`, Ni_4Ti_3
	775	1321 ± 13	151 ± 2	Ni_3Ti, Ti_2Ni, B2, B19`, Ni_4Ti_3
KTF639 500 W 2 mTorr	As-deposited	1040 ± 14	151 ± 2	Amorphous
	550	614 ± 6	88 ± 1	B2, B19`
	700	655 ± 2	163 ± 1	Ni_3Ti, Ti_2Ni, B2, B19`
	775	558 ± 7	88 ± 1	B2, Ti_2Ni, B19`, Ni_4Ti_3
KTF640 300 W 7,5 mTorr	As-deposited	868 ± 6	141 ± 1	Amorphous
	550	990 ± 7	138 ± 1	B2, Ti_2Ni, B19`
	700	1560 ± 18	172 ± 2	Ti_2Ni, Ni_3Ti, Ni_4Ti_3
	775	1100 ± 8	137 ± 1	B2, Ti_2Ni
KTF641 500 W 7,5 mTorr	As-deposited	905 ± 4	133 ± 1	Amorphous
	550	755 ± 9	107 ± 1	B2, B19`, Ti_2Ni
	700	587 ± 8	99 ± 1	B2, B19`, Ti_2Ni
	775	510 ± 9	48 ± 1	B19`, B2, Ti_2Ni

For the film produced at 300 W- 2 mTorr, hardness decreased when the film annealed at 550 °C. Increasing annealing temperature resulted with the increase in the hardness of the film due to the formation of precipitates after crystallization. NiTi film produced at 500 W- 2 mTorr, showed decrease in hardness when annealed at 550 °C. Hardness increased when annealed at 700 °C as the result of precipitate formation. However, after annealing at 775 °C, hardness decreased again due to the formation of B2 austenitic phase as the major phase near precipitates.

For the film produced at 300 W- 7,5 mTorr, hardness increased when annealed at 550 °C. This was the result of formation of B2 phase as the major phase and Ti_2Ni and B19` as the minor phases. Formation of precipitates as the main phases when annealed at 700 °C, increased the hardness of the film. However, hardness of the film decreased again after the formation of B2 austenite phase as the major phase when annealed at 775 °C. For the film produced at 500 W- 7,5 mTorr, hardness decreased with increasing annealing temperature. The reason for this was the formation of B19` martensitic phase as the major phase with increasing annealing temperature. Among all the films, the last one produced at 500 W- 7,5 mTorr showed the lowest hardness due to rare formation of second phase precipitates which give high hardness to the film structure.

Yerli worked on the hardness of NiTi films, but only for the as-deposited films produced at 250 W and % 100 Ar atmosphere. He found the hardness of as-deposited film 853 HV [59]. Any other study about hardness of crystallized NiTi films was not present in the literature.

6.3.2. Thickness Measurements with XRF

Thickness of the films deposited under different deposition conditions were determined with XRF method. The results were verified by using Semafore 3.01 software on cross-sectional SEM micrographs of the films as shown in Table 6.3.

Table 6.3 Thickness of the films determined by XRF and cross-sectional SEM micrographs

Samples	Thickness (μm)	
	XRF	SEM
KTF638 (300 W- 2 mTorr)	1,32	1,38
KTF639 (500W- 2 mTorr)	3,20	3,25
KTF640 (300 W- 7,5 mTorr)	2,20	2,24
KTF641 (500W- 7,5 mTorr)	3,44	3,58

Thickness of the films showed that both target power and partial Ar pressure were affecting the thickness of the films. However, the difference between the values or the increasing percent of the thickness values showed that target power was more effective than partial Ar pressure on the thickness of the films. Ishida and Sato [60] studied on the effect of film thickness on shape memory behavior of the Ti-50 at.% Ni films by depositing films with varying thickness. However, in their study, beside

the constant deposition parameters, only time was changed to obtain different thickness values. They found that effect of film thickness on shape memory behavior became prominent below 5 μm and negligible above 5 μm. Besides, they reported that surface oxidation also affected the TTRs when the thickness was less than 1 μm. In our study, the maximum thickness value was about 3,5 μm. Deposition parameters were changed to examine their effects on deposited films in terms of crystallization and shape memory behavior. Because the deposition parameters were changed in this study, the reason for the differences in transformation behavior of the films was questionable whether it was the changed deposition parameters or the thickness.

6.3.3. Cross-sectional SEM Analyses

Cross-sectional morphologies of as-deposited films and films annealed at different temperatures were examined with Jeol JSM-5410 Scanning Electron Microscope. Figure 6.10 shows cross-sectional micrographs of KTF638 films. There can be

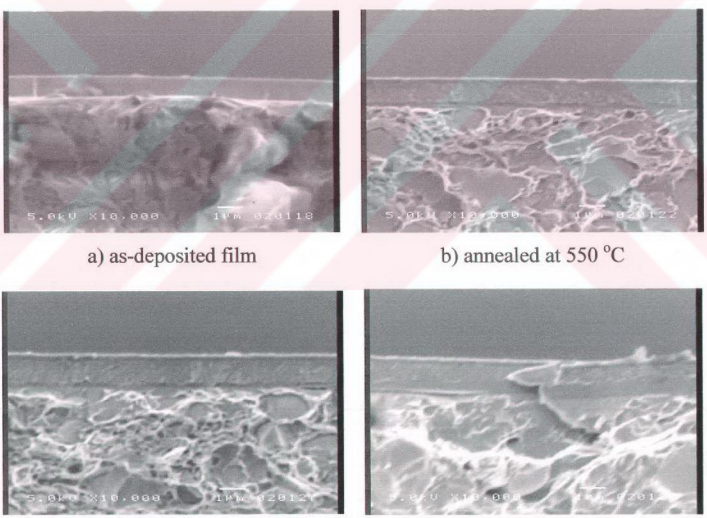

a) as-deposited film b) annealed at 550 °C

c) annealed at 700 °C d) annealed at 775 °C

Figure 6.10 Cross-sectional micrographs of KTF638 film produced at 300W- 2 mTorr P_{Ar}.

noticed a significant difference between the as-deposited and crystallized films. The morphologies of as-deposited films were thought as featureless. After annealing, the

films were crystallized and cross-sectional morphologies changed from featureless to near featureless. There were some local zones exhibiting the columnar structure.

Cross-sectional micrographs belonging to KTF639 films did not show any significant difference between as-deposited and annealed films as shown in Figure 6.11. But here, a thin oxide layer on the film surface can be noticed. This layer was also noticed by naked eye due to the alteration of the surface color. But XRD patterns did not show any peaks exhibiting oxide phase for which was thought to be found in amorphous state.

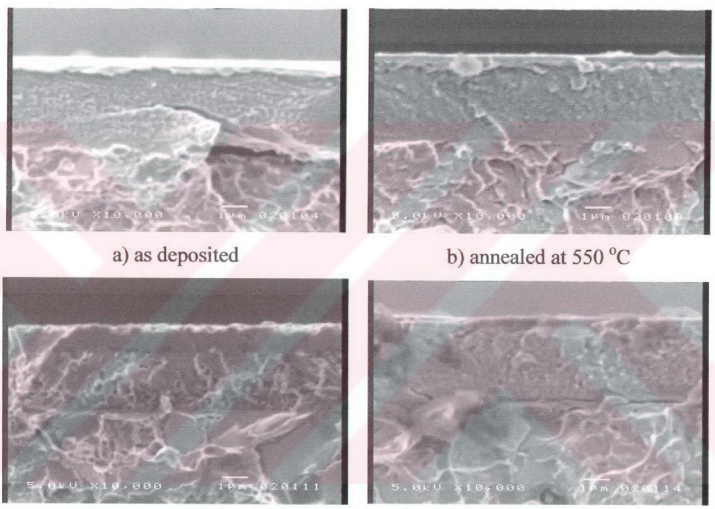

a) as deposited b) annealed at 550 °C

c) annealed at 700 °C d) annealed at 775 °C

Figure 6.11 Cross-sectional micrographs of KTF639 film produced at 500W- 2 mTorr P_{Ar}.

The cross sectional morphologies of KTF 640 films for as-deposited and annealed states are shown in Figure 6.12. For all of them two different zones were present through the middle of the cross-section and they all showed different fracture types, Especially, the film annealed at 775 °C showed a structure which was looking like a herringbone.

Figure 6.13 shows the micrographs belonging to KTF641 films. Thin oxide layer about 0,1 μm was present again on the top of the film surfaces. Near featureless

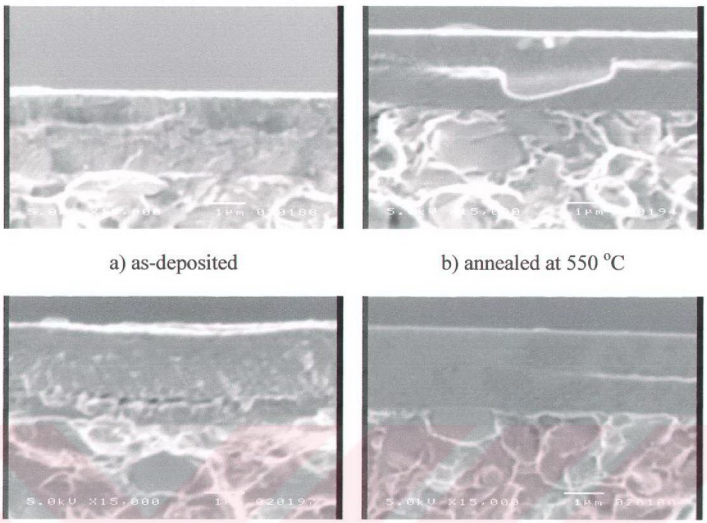

a) as-deposited b) annealed at 550 °C

c) annealed at 700 °C d) annealed at 775 °C

Figure 6.12 Cross-sectional micrographs of KTF 640 film produced at 300W- 7,5 mTorr P_{Ar}.

structure was seen in as-deposited film and for the film annealed at 550 °C changed to featureless type in the film annealed at 700 °C. Finally the film showed the columnar structure when annealed at 775 °C.

According to Miyazaki and Ishida [57], the films prepared at low Ar pressure exhibited a flat and featureless structure, while films prepared at high Ar pressure exhibited a columnar structure which showed the films were porous. This structure seemed to be caused by the restricted mobility of deposited atoms on the surface of the films. Thus, a high Ar gas pressure was likely to decrease the energy of the sputtered atoms by collision with Ar atoms. Furthermore, under a high Ar gas pressure, Ar ions adsorbed on the film surface could interfere with the surface diffusion of sputtered Ti and Ni atoms. Thus, the films deposited under high Ar pressure (7,5 mTorr) showed columnar structure even if they were not clearly noticeable for most of them.

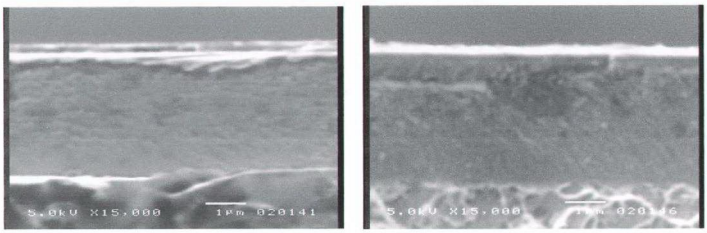

a) as-deposited b) annealed at 550 °C

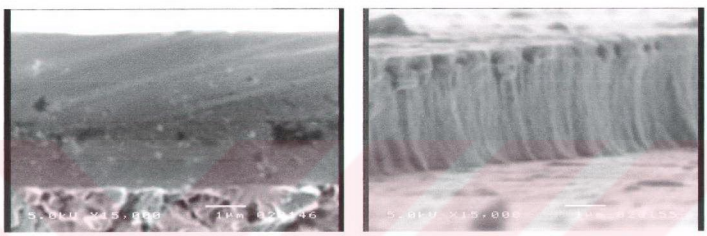

c) annealed at 700 °C d) annealed at 775 °C

Figure 6.13 Cross-sectional micrographs of KTF 641 film produced at 500W- 7,5 mTorr P_{Ar}.

7. CONCLUSION

1. It was possible to deposit NiTi thin films on HSS substrates with DC magnetron sputtering method under varying sputtering conditions.
2. Because the as-deposited films were amorphous, they were annealed at three different temperatures of 550, 700 and 775 °C under high vacuum. Films crystallized in different phase formations depending on the annealing temperatures.
3. Ti content of the films increased with increasing target power and argon pressure. The highest Ti content was obtained as 58,9 at. % for the film produced at 500 W- 7,5 mTorr.
4. Present phases and transformation properties of the films were determined with XRD method. All as-deposited films showed amorphous structure. Films annealed at different temperatures of 550, 700 and 775 °C resulted with different crystallization behaviors.
5. Films annealed at 700 °C showed the crystallization of second phase Ti_2Ni, Ni_3Ti and Ni_4Ti_3 precipitates as the major phases. With varying amounts, annealing at 550 and 775 °C showed formation of B2 austenitic and B19` martensitic phases as the major phases with second phase precipitates beside them.
6. Films produced at 500 W- 7,5 mTorr, increasing annealing temparature resulted with the formation of B19` martensitic phase as the major phase instead of austenitic phase. Transformation experiment of film at 70 °C verified this result. It was also determined qualitatively that TTRs of this film is the highest one among all produced films due to presence of B19` martensite as the major phase at room temperature.
7. When annealed at 550 °C, with the formation of sharp and intensive peaks, films produced at 500 W showed better crystallization than the ones

produced at 300 W. Films produced at 2 mTorr showed Ni_3Ti precipitate as the major phase when annealed at 700 °C whereas the films produced at 7,5 mTorr tended to form Ti_2Ni precipitate as the major phase for the same annealing temperature.

8. Peaks belonged to B2 and B19` phases shifted from their original peak positions. The reason for this was the residual stress existing in the film structures.

9. Hardness of the films were measured and evaluated with the present phases in the film structures. Films resulted thr crystallization of second phase precipitates as the major phases showed the highest hardness. With the formation of B2 austenitic and B19` martensitic phases, the hardness of the films tended to decrease. The highest hardness obtained as 1560 HV for the film produced at 300 W- 7,5 mTorr and annealed at 700 °C. The present phases for this film were the second phase precipitates. The lowest hardness obtained as 510 HV for the film produced at 500 W- 7,5 mTorr and annealed at 775 °C.

10. The thickness of the films were measured with XRF method based on emission principal which is related with the x-rays generated by the film. The thickness of the films were also determined from the cross-sectional micrographs using the Semafore 3.01 software and the results were compatible with each other. The highest thickness obtained about 3,5 μm for the film produced at 500 W- 7,5 mTorr indicating that increase in target power and argon pressure increased the film thickness.

11. Cross-section morphologies did not show significant results for the films to be compared with each other in terms of sputtering and annealing conditions. However, the film produced at 500 W- 7,5 mTorr and annealed at 775 °C showed columnar structure with increase in argon pressure which can be harmonized with the formation of B19` martensite phase when compared to the films produced at 2 mTorr.

REFERENCES

[1] **Tabanlı, M. R.,** 2000. Fatigue and Fracture of Nickel-Titanium, *Ph.D. Thesis*, University of Miami, Coral Gables, Florida.

[2] **Wayman, C.M. and Duerig, T.W.,** 1990. An Introduction to Martensite and Shape Memory, in: *Engineering Aspects of Shape Memory Alloys*, pp. 3-20, eds. Duerig, T.W., Melton, K.N., Stöckel, D. and Wayman, Butterworth-Heinemann

[3] **Otsuka, K. and Wayman, C.M.,**1998. Introduction, in: *Shape Memory Materials*, pp. 1-26, eds. Otsuka, K. and Wayman, C.M., Cambridge University Press

[4] Two-Way Memory, www.sma-inc.com/twoway.html

[5] Shape Memory Alloys, www.sma-inc.com/SMAPaper.html

[6] Introduction to Shape Memory and Superelasticity , www.sma-inc.com / SMAandSE.html

[7] **Barnes, C.,** Shape memory and Superelastic Alloys, http://innovations.copper.org/1999/07/shape.html,

[8] **Melton, K.N.,** 1990. NiTi Based Shape Memory Alloys, in: *Engineering Aspects of Shape Memory Alloys*, pp. 21- 35, eds. Duerig, T. W., Melton K.N., Stöckel, D. and Wayman, Butterworth-Heinemann

[9] **Ho, K.K.,** 2001. Sputter Deposition and Characterization of Thin Film Nickel Titanium Shape Memory Alloy For Microelectromechanical Systems Application. *Ph.D. Thesis*, University of California, Los Angeles.

[10] **Zhang, C.,** 2000. NiTi and NiTiHf Shape Memory Thin Films. *Ph.D. Thesis*, Auburn University, Auburn, Alabama.

[11] **Gill, J.J.,** 2001. Thin Film NiTi Shape Memory Alloy Microactuators. *Ph.D. Thesis*, University of California, Los Angeles.

[12] **Zhang, J.,** 1997. Stress Evolution During Isothermal and Isochronal Annealing of Sputtered NiTi Thin Films on (100)-Si. *M.Sc.Thesis*, Michigan State University, Michigan.

[13] **Ho, K, Carman, G.P., and Jardine. P.,** 1999. Sputter Deposition of NiTi Thin Film Exhibiting the SME at Room Temperatures, *SPIE Smart Structures Conference*, **V 3675**, pp. 252-267.

[14] **Fu, Y. and Du, H.,** 2002. RF Magnetron Sputtered TiNiCu Shape Memory Alloy Thin Film, *Material Science & Engineering*, Article in Press, **A00**, 1-7

[15] **Ho, K., Gill, J., and Carman G.P.,** 1999. Sputter Deposited NiTi Thin Film SMA for Active Flow Control, *10th International Conference on Adaptive Structures*, pp. 197-208.

[16] **Ho, K. K. and Carman, G. P.,** 2000. Sputter Deposition of NiTi Thin Film Shape Memory Alloy Using a Heated Target, *Thin Solid Films*, **370**, 18-29.

[17] **Ho, K. H., Mohanchandra, K. P. and Carman, G. P.,** 2002. Examination of the Sputtering Profile of NiTi Under Target Heating Conditions, *Thin Solid Films*, **413**, 1-7

[18] Glossary of NiTi Terminology, www.sma-inc.com/glossary.html

[19] **Shimizu, K. and Tadaki, T.**, 1984. Shape Memeory Effect: Mechanism, in: *Shape Memory Alloys, pp. 1-36, eds. Funakubo, H.* Sangyo Tosho K.K., Tokyo

[20] **Mendelson, S.,** 1975. Mechanisms for the martensite formation and the shape memory effect, in: *Shape Memory Effects in Alloys*, Perkins, J., Plenum Press, New York London

[21] **Otsuka, K. and Wayman, C.M.,**1998. Mechanism of Shape Memory Effect and Superelasticity, in: *Shape Memory Materials*, pp. 27-48, eds. Otsuka, K. and Wayman, C.M., Cambridge University Press

[22] **Huang, X and Liu, Y.,** 2001. Effect of annealing on the transformation behaviour and superelasticity of NiTi shape memory alloy. *Scripta Materialia*, **45**, 153-60

[23] **Wang, Z., Zu, X.,, Feng, X and Dia J.,** 2000. Effect of thermomechanical treatment on the two-way shape memory effect of NiTi alloy spring, *Materials Letter*, **54** , 55-61

[24] **Perkins, J. and Hodgson, D.,** 1990. The Two Way Shape Memory Effect, in: *Engineering Aspects of Shape Memory Alloys*, pp. 182-195, eds. Duerig, T.W., Melton, K.N., Stöckel, D. and Wayman, Butterworth-Heinemann.

[25] **Sauthoff, G.,** 1995. NiTi, in: *Intermetallics*, Weinheim – New York.

[26] **Winzek, B.,** 2000. Entwicklung, Herstellung und Charakterisierung von Mikroaktoren mit Formgedächtnisschichten auf der Basis vın TiNi, *Ph.D. Thesis*, der Univeristät Karlsruhe, Karlsruhe.

[27] **He, J.L., Won, K.W. and Chang, J.T.,** 2000. TiNi thin films prepared by cathodic arc plasma ion plating, *Thin Solid Films*, **359**, 46-54

[28] **Saburi, T.,**1998. TiNi Shape Memory Alloys, in: *Shape Memory Materials*, pp. 49-96, eds. Otsuka, K. and Wayman, C.M., Cambridge University Press

[29] **Hornbogen, E., Mertinger, V., and Wurzel, D.,** 2001. Microstructure and Tensile Properties of two binary NiTi Alloys. *Scripta Materialia*, **44**, 171-178

[30] **Joint Committee on Powder Diffraction Standards,** 1994. Powder Diffraction file, *International Center for Diffraction Data*. Park Lane.

[31] **Perkins, J. and Hodgson, D.,** 1990. The Two Way Shape Memory Effect, in : *Engineering Aspects of Shape Memory Alloys*, pp. 182-195, eds. Duerig, T.W., Melton, K.N., Stöckel, D. and Wayman, Butterworth-Heinemann

[32] **Uchil, J., Kumara K.G. and Mahesh, K.K.,** 2002. Effect of Thermal Cycling on R-Phase stability in a NiTi Shape Memory Alloy, *Materials Science and Engineering*, **332**, 25-28

[33] **Uchil, J., Mohanchandra, K.P., Mahesh, K.K. and Kumara K.G.,** 1998. Thermal and Electrical Characterization of R-Phase dependence on heat-treat temperature in Nitinol, *Physica*, **253**, 83-89

[34] **Stróz, D.,** 2003. TEM studies of the R-phase transformation in a NiTi shape memory alloy after thermo-mechanical treatment, Article in Press, *Materials Chemistry and Physics*, **9807**, 1-3.

[35] Selected Properties of NiTi, http://www.sma-inc.com/html/ selected_properties. html

[36] Measuring Transformation Temperatures in NiTi Alloys, http://www.sma-inc.com/ttrmeas.html

[37] **Suzuki, Y.** 1998. Fabrication of Shape Memory Alloys, in: *Shape Memory Materials*, pp. 133-148, eds. Otsuka, K. and Wayman, C.M., Cambridge University Press

[38] **Brantley, W.A.,** Iijima, M., and Grentzer, T.H., 2002. Temperature-modulated DSC study of phase transformations in nickel-titanium orthodontic wires. *Thermochimica Acta*, **392-393**, 329-337.

[39] **Harrison, J. D.,** 1990. Measurable Changes Concomitant with the Shape Memory Effect Transformation, in: *Engineering Aspects of Shape Memory Alloys*, pp. 106-114, eds. Duerig, T.W., Melton, K.N., Stöckel, D. and Wayman, Butterworth-Heinemann

[40] **Starosvetsky, D., and Gotman, I.**, 2001. Corrosion behavior of titanium nitride coated Ni-Ti shape memory surgical alloy. *Biomaterials*, **22**, 1853-1859

[41] **He, J.L., Won, K.W., Chang, C.T., Chen, K.C., and Lin H.C.,** 1999. Cavitation-resistant TiNi films deposited by using cathodic arc plasma ion plating. *Wear*, **233-235**, 104-110.

[42] **Miyazaki, S.,** 1998. Medical and Dental Applications of Shape memory Alloys, in: *Shape Memory Materials*, pp. 267-281, eds. Otsuka, K. and Wayman, C.M., Cambridge University Press

[43] **Hsieh, S.F., Wu, S.K., and Lin, H.C.,** 2002. Martensitic transformation of a Ti-rich, Ti51Ni47Si2 shape memory alloy. *Journal of Alloys and Compounds*, **335**, 254-261.

[44] Applications of Shape Memory and Superelastic Alloys, http://www.sma-inc.com /Applications.html

[45] **Surbled, P., Clerc, C., Le Pioufle, B., Ataka, M., and Fujita, H.,** 2001. Effect of the composition and thermal annealing on the transformation temperatures of sputtered TiNi shape memory alloy thin films. *Thin Solid Films*, **401**, 52-59

[46] **Goldberg, F., and Knystautas, E.J.,** 1996. NiTi thin film characterization by Rutherford backscattering spectrometry. *Materials Science and Engineering*, **B40**, 185-189.

[47] **Bendehan, M., Seguin, J.L., Canet, P., and Carchano,** H., 1996. NiTi shape memory alloy thin films: composition control using optical emission spectrometry, *Thin Solid Films*, **283**, 61-66.

[48] **Frantz, N., Gergam, E.D., Grandchamp., Bosseboeuf, A., Seiler, W., Nouet., G., and Catillon, G.,** 2002. Shape memory thin films with transition above room temperature from Ni-rich NiTi films. *Sensors and Actuators*, **A99**, 59-63.

[49] **Büttgenbach, S., Bütefisch, S., Schädel, M.L., and Wogersien, A.,** 2001. Shape memory microactuators, *Microsystem Technologies*, **7**, 165-170.

[50] **Seguin, J.L., Bendehan, M., Isalgue, A., Cano, V.E., Carchano, H., and Torra, V.,** 1999. Low temperature crystallized Ti-rich NiTi shape memory alloy films for microactuators, *Sensors and Actuators*, **74**, 65-69

[51] **Huang, W.,** 2002. On the selection of shape memory alloys for actuators, *Materials and Design*, **23**, 11-19.

[52] **Fu, Y., Huang, W., Du, H., Huang, X., Tan, J, and Gao, X.,** 2001. Characterization of NiTi shape memory alloy thin films for MEMS applications. *Surface Coatings and Technology*, **145**, 107-112.

[53] **Materials Research Corporation**, *The Basics of sputtering*, 3rd edition, Orangeburg, New York.

[54] **Musil, J., and Vlcek, J.,** 1999. A perspective of magnetron sputtering in surface engineering., *Surface and Coatings Technology*, **112**, 162-169.

[55] **Fu, Y., and Du, H.,** 2003. Effects of film composition and annealing on residual stress evolution for shape memory TiNi film., *Materials Science and Engineering A*, **342**, 236-244.

[56] **Yang, Y.Q., Jia, H.S., Zhang, Z.F., Shen, H.M., Hu, A. And Wang, Y.N.,** 1995. Transformations in sputter-deposited thin films of NiTi shape memory alloy, *Materials Letters*, **22**, 137-140.

[57] **Miyazaki, S. and Ishida, A.,** 1999. Martensitic transformation and shape memory behavior in sputter-deposited TiNi-base thin films. *Materials Science and Engineering A*, **273-275**, 106-133.

[58] **Huang, X. And Liu, Y.,** 2003. Substrate-induced stress and the transformation behavior of sputter deposited NiTi thin films. *Materials Science and Engineering A*, **352**, 314-317.

[59] **Yerli, Z.Ö.,** 2002. Wear Behaviors of NiTi films produced with magnetron sputtering, *B. Sc. Thesis*, Istanbul Technical University, Istanbul.

[60] **Ishida, A., and Sato, M.,** 2003. Thickness effect on shape memory behavior of Ti-50,0 at.%Ni thin film. *Acta Materialia*, **51**, 5571-5578.

APPENDIX A

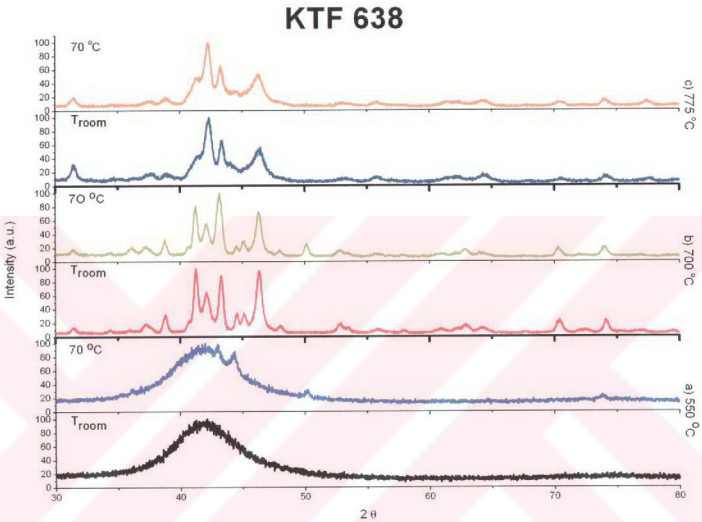

Figure A.1 Transformation experiments of KTF638 (300 W – 2 mTorr) films at 70 °C for different annealing temperatures.

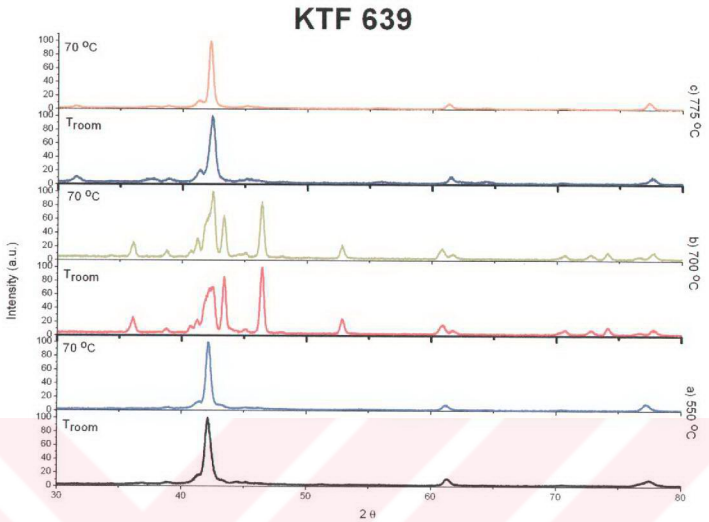

Figure A.2 Transformation experiments of KTF639 (500 W – 2 mTorr) films at 70 °C for different annealing temperatures.

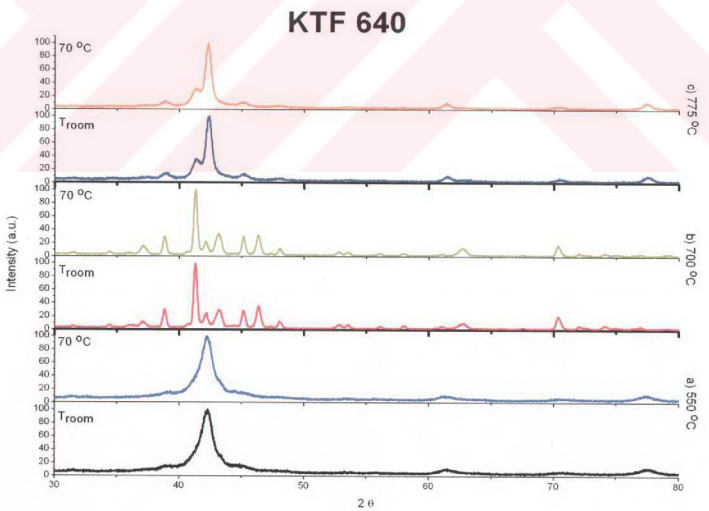

Figure A.3 Transformation experiments of KTF640 films (300 W- 7,5 mTorr) at 70 °C for different annealing temperatures.

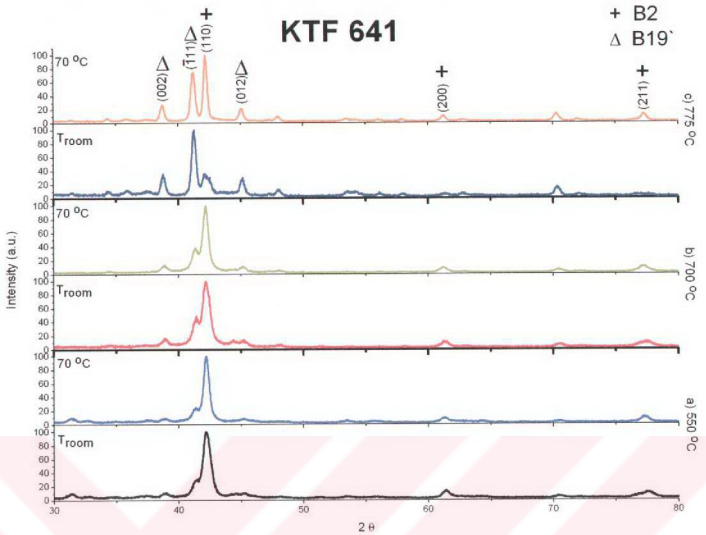

Figure A.4 Transformation experiments of KTF641 (500 W- 7,5 mTorr) films at 70 °C for different annealing temperatures.

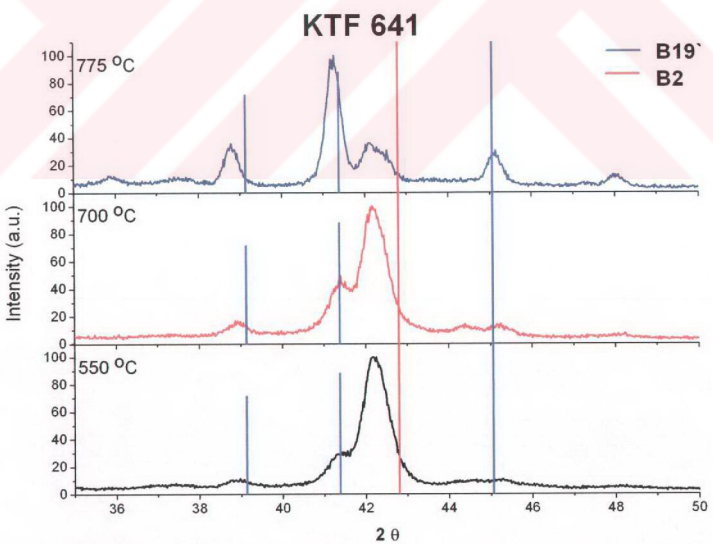

Figure A.5 Magnified scheme of XRD patterns of KTF 641 (500 W- 7,5 mTorr) films compared with the original peak positions of B2 and B19` phases.

APPENDIX B

Table B.1 JCPDS of NiTi with Reference File No of 18-0899 [30].

18-899 JCPDS-ICDD Copyright 1994

NiTi

Nickel Titanium / austenite

Rad: CuK_{α} Lambda: 1.54050 Filter: Ni d-sp: D.S. -114.6
Cutoff: Int: I/Icor:
Ref: Dwight, Private Communication, (1965)

Sys: Cubic S.G.: Pm3m (221)
a: 2.998 b: c: A: C:
A: B: C: Z: 1 mp:
Ref: Dwight, Trans. Am. Inst. Min. Eng., 215 283 (1959)

Dx: 6.569 Dm: SS/FOM: F7=5(.104,13)

2-theta	Int.	h k l
42.803	100	1 1 0
61.982	40	2 0 0
78.153	60	2 1 1
93.335	10	2 2 0
108.692	30	3 1 0
125.877	20	2 2 2
148.071	70	3 2 1

Table B.2 JCPDS of NiTi with Reference File No of 19-0850 [30].

19-850 JCPDS-ICDD Copyright 1994

NiTi

Nickel Titanium / austenite

Rad: CoK_{α} Lambda: 1.7902 Filter: d-sp: Guinier
Cutoff: 1.3 Int: Visual I/Icor:
Ref: Hughes, J. Iron Steel Inst., London, 203 1019 (1965)

Sys: Cubic S.G.: Pm3m (221)
a: 2.972 b: c: A: C:
A: B: C: Z: 1 mp:
Ref: Ibid.

Dx: 6.743 Dm: SS/FOM: F4=236(.004,4)

2-theta	Int.	h k l
30.044	5	1 0 0
42.995	100	1 1 0
53.345	5	1 1 1
62.446	50	2 0 0

Table B.3 JCPDS of NiTi with Reference File No of 35-1281 [30].

35-1281 JCPDS-ICDD Copyright 1994

NiTi

Nickel Titanium / martensite

Rad: CuK_α Lambda: 1.54178 Filter: d-sp: Diff.
Cutoff: Int: Diffractometer I/Icor:
Ref: Michal, G., Sinclair, Acta Crystallogr., Sec. B, 37 1803 (1981)

Sys: Monoclinic S.G.: P21/m (11)
a: 2.885(4) b: 4.622(5) c: 4.120(5) A: C:
A: B: C: 96.8(1) Z: 2 mp:
Ref: Ibid.

Dx: 6.490 Dm: SS/FOM: F21=115(.009,21)

2-theta	Int.	h k l	2-theta	Int.	h k l
19.322	6	0 1 0	54.830	<1	1 0 2
29.102	1	0 1 1	57.285	5	1 -1 2
31.194	<1	1 0 0	58.847	1	1 2 1
34.882	13	1 -1 0	60.112	1	1 1 2
38.235	11	1 0 1	60.328	26	0 2 2
38.941	2	1 1 0	60.459	1	0 3 0
39.223	54	0 2 0			
41.365	100	1 -1 1			
43.917	54	0 0 2			
44.927	94	1 1 1			
45.187	26	0 2 1			
47.728	1	1 -2 0			
48.404	<1	0 1 2			
52.946	8	1 -2 1			
54.025	<1	1 2 0			

Table B.4 JCPDS of NiTi with Reference File No of 27-0344 [30].

27-344 JCPDS-ICDD Copyright 1994

NiTi

Nickel Titanium / martensite

Rad: CuK_{α} Lambda: 1.5418 Filter: Ni d-sp:
Cutoff: Int: Diffractometer I/Icor:
Ref: Otsuka et al., Phys. Status Solidi A, 5 457 (1971)

Sys: Monoclinic S.G.: P21/m (11)
a: 2.889 b: 4.120 c: 4.622 A: C:
A: B: 96.8 C: Z: 2 mp:
Ref: Ibid.

Dx: 6.481 Dm: SS/FOM: F8=5(.073,21)

2-theta	Int.	h k l
19.280	15	0 0 1
38.439	18	1 1 0
39.135	65	0 0 2
41.385	80	-1 1 1
43.917	55	0 2 0
45.068	100	0 1 2
52.880	12	-1 1 2
60.459	25	0 0 3

Table B.5 JCPDS of Ti_2Ni with Reference File No of 18-0898 [30].

18-898 JCPDS-ICDD Copyright 1994

Ti_2Ni

Nickel Titanium

Rad: CoK_α Lambda: 1.7902 Filter: d-sp:
Cutoff: Int: Diffractometer I/Icor:
Ref: Yurko, Barton, Parr, Acta Crystallogr., 12 909 (1959)

Sys: Cubic S.G.: Fd3m (227)
a: 11.278 b: c: A: C:
A: B: C: Z: 32 mp:
Ref: Ibid.

Dx: 5.723 Dm: 5.723 SS/FOM: F30=37(.021,40)

2-theta	Int.	h k l	2-theta	Int.	h k l
13.591	10	1 1 1	63.300	6	5 5 3
22.263	2	2 2 0	66.229	2	8 0 0
27.335	6	2 2 2	67.973	2	7 3 3
31.704	2	4 0 0	70.846	25	6 6 0
34.646	4	3 3 1	72.545	10	7 5 1
39.099	30	4 2 2	73.066	2	6 6 2
41.564	100	5 1 1	76.956	6	9 1 1
45.450	30	4 4 0	77.475	8	8 4 2
47.675	6	5 3 1			
48.376	8	4 4 2			
53.212	2	5 3 3			
53.888	2	6 2 2			
56.479	4	4 4 4			
58.397	4	5 5 1			
61.481	2	6 4 2			

Table B.6 JCPDS of Ni_3Ti with Reference File No of 05-0723 [30].

5- 723 JCPDS-ICDD Copyright 1994

Ni_3Ti

Nickel Titanium

Rad: CoK_α Lambda: 1.7890 Filter: d-sp:
Cutoff: Int: I/Icor:
Ref: Duwez, Taylor, J. Met., 188 1173 (1950)

Sys: Hexagonal S.G.: P63/mmc (194)
a: 5.093 b: c: 8.32 A: C: 1.6336
A: B: C: Z: 4 mp:
Ref: Ibid.

Dx: 7.961 Dm: SS/FOM: F22=2(.195,65)

2-theta	Int.	h k l
20.212	10	1 0 0
22.783	10	1 0 1
35.023	10	1 1 0
40.798	20	2 0 0
42.402	50	2 0 1
43.694	50	0 0 4
46.535	100	2 0 2
53.212	20	2 0 3
60.026	10	2 1 2
61.345	20	2 0 4
70.785	20	2 0 5
74.268	50	2 2 0

Table B.7 JCPDS of Ni_4Ti_3 with Reference File No of 39-1113 [30].

39-1113 JCPDS-ICDD Copyright 1994

Ni_4Ti_3

Nickel Titanium

Rad: CuK_α Lambda: 1.5405 Filter: Ni d-sp: Diff.
Cutoff: Int: Visual I/Icor:
Ref: Saburi, T., Osaka University, Osaka, Japan, Private Communication, (1987)

Sys: Rhombohedral (Hex) S.G.: R3 (146)
a: 11.235 b: c: 5.0789 A: C: .4521
A: B: C: Z: mp:
Ref: Saburi, T., Nenno, S., Fukuda, T., J. Less-Common Met., 125 157 (1986)

Dx: Dm: SS/FOM: F7=2(.071,43)

2-theta	Int.	h k l
37.637	30	1 3 1
40.134	15	2 0 2
43.211	100	1 2 2
49.355	20	3 1 2
54.759	15	2 3 2
62.306	20	4 2 2
78.306	20	5 3 2

RESUME

Ş. Murat TELLİ was born in İstanbul in 1979. After graduating from Kültür Fen Lisesi in 1996, he started to under graduate education at İstanbul Technical University in the department of Materials and Metallurgical Engineering in 1997. He graduated from this department in 2001, and in the following year, he was accepted to Materials Science and Engineering Department of Advanced Technologies in Engineering Graduate Programme in İstanbul Technical University and he is still continuing his studies in the same department.